Received: 22 September 2015 | Revised: 22 June 2020 | Accepted: 29 June 2020

DOI: 10.1002/oca.2662

RESEARCH ARTICLE

WILEY

Finite horizon nonlinear optimal control for a quadrotor: Experimental results

Omar Santos-Sánchez[1] | **Orlando García**[1] | **Hugo Romero**[1] | **Sergio Salazar**[2] | **Rogelio Lozano**[3]

[1]Information Technologies and Systems Research Center, UAEH, Pachuca, Mexico

[2]UMI Cinvestav, CDMX, Mexico City, Mexico

[3]DR CNRS Sorbonne Universitiés, Université de Technologie de Compiègne, CNRS, Compiègne, France

Correspondence
Sergio Salazar is with UMI Cinvestav, CDMX México AP 14-470, Mexico.
Email: sesalazar@cinvestav.mx

Summary

In this article, a suboptimal nonlinear discrete control sequence for nonlinear discrete affine control systems is proposed. **Using the dynamic programming approach in discrete time domain, the suboptimal control sequence is obtained in every step considering a quadratic performance index of finite horizon**. The proposed control strategy is applied to improve the dynamic and energetic performances of a quadrotor unmanned aerial vehicle, when it is subject to special maneuvers or flight conditions, such as the take off and landing phases or trajectory tracking. For these tasks, it could be required convergence in finite time and good behavior. Performing a comparative experimental study with others controllers (optimal linear and PD controllers), the effectiveness of proposed approach is proven.

KEYWORDS

discrete optimal control, energetic performances, quadrotor

1 | INTRODUCTION

Unmanned aerial vehicles (UAVs) have been an engaging research topic in the last years. Many control algorithms and different applications with UAVs have been widely reported. The optimal control approach is one of these control strategies, which has been studied and applied to quadrotors. In fact, some applications requires special maneuvers to achieve a specific behavior in a finite time with minimal energy. Some examples are the take off and landing phases, together with collision avoidance and tracking trajectories tasks. In the case of Reference 1, the optimal control is applied to quadrotors, the Pontryaguin's principle was used in order to obtain the optimal inputs, which were applied to the model of the quadrotor to perform maneuvers between two different states. Based on time optimal problem, experimental results were performed. In Reference 2, an hexarotor was studied, the continuous optimal control was obtained to solve the tracking problem for the UAV, a linear model was considered, and a robust component was added to optimal control problem. This was done in order to give a certain degree of robustness to the aerial platform under tracking errors. Satisfactory simulation and experimental results were presented. In Reference 3, a continuous linear quadratic regulator (LQR) was applied to control the longitudinal flight motion of a UAV P15035. The LQR controller was combined with a Kalman estimator using the separation principle for the altitude control. Simulation results show some improvements compared with classical design.

Furthermore, in Reference 4, a method for learning and online generalization of maneuvers for quadrotor-type vehicles was presented. The maneuvers were formulated as continuous optimal control problems, and the optimal solutions

were encoded and generalized with dynamic movement primitives. Satisfactory simulation and experimental results were presented. The differential flatness approach was used in Reference 5 to propose a continuous optimal feedback control algorithm for any system having the flatness property using an asymptotically optimal algorithm based on rapidly expanding random trees. The proposed algorithm was applied to a quadrotor model considering different maneuvers, simulation results were exposed. In Reference 6, a model and continuous optimal control were synthesized, and the model considers some aspects as vortex ring state or blade flapping and the gyroscopic effect produced by the rotors. A control based on the LQR approach was tested in a linear version on the proposed model and simulation results were exposed in order to show the feasibility of the proposed model. In Reference 7, a L_1-optimal control of a quadrotor was presented, due that the existence of noise in the measured variable, the proposed controller was synthesized minimizing the L_∞ gain of the plant with respect to disturbances. The performance of the proposed controller was evaluated in simulation and experimental results, and it was compared to a robust nonlinear controller given in the literature.

A backstepping approach based on a continuous inverse optimal attitude controller was proposed to drive a quadrotor helicopter is proposed in Reference 8. This controller has the property of the maximum convergence according with a control Lyapunov function, the backstepping approach allows to handle the complexity introduced by the use of the unit quaternion representation; in order to avoid to solve the Hamilton Jacobi Bellman (HJB) equation, an inverse optimal approach was also used, the performance of the proposed controller is compared with a PD controller in an experimental platform (quadrotor). Furthermore, in Reference 9, the design, construction, and implementation of an unmanned rotorcraft (quadrotor helicopter) were presented, that platform allows the motion control of the pitch, roll, and yaw angles. The tested controllers were a discrete PID control law and discrete LQR scheme, additionally a Kalman filter was used to estimate the angular rates. The attitude control law behavior was experimentally tested, obtained an acceptable performance. A comparison between PID, LQR, and nonlinear controllers (adaptive integral backstepping controller) was presented in Reference 10, in that article a nonlinear control approach was proposed, this control law is based on a recursive Lyapunov methodology using the backstepping technique and an adaptive scheme. Satisfactory simulations and real-time experiments were conducted. The authors of Reference 11 present an LQR approach to stabilize the attitude and altitude of an octorotor. Numerical simulations have demonstrated the effectiveness of that control strategy under nominal conditions. Moreover, the authors improved the LQR results by adding the integral action to the altitude controller. In Reference 12, an LQR methodology and integral state augmentation were adopted in order to achieve the desired control system performance, and the unmeasured states are estimated by a reduced-order observer. Satisfactory simulation results on the UAV helicopter were reported. Summarizing those previous works, for continuous time domain the reported results use linear models, the LQR approach, or continuous nonlinear controllers. However, for a digital implementation, it could be useful to obtain a discrete nonlinear controller.

In Reference 13, a nonlinear discrete suboptimal control was proposed for time delay systems in the state and input, although the dynamic programming approach was used on a different plant and experimental platform (stable plant were considered). In Reference 14, an iterative two-stage dual heuristic programming (DHP) was proposed to solve the infinite horizon optimal control problems for a class of discrete-time switched nonlinear systems subject to actuators saturation. The iterative two-stage DHP algorithm was developed to solve the HJB equation of the switched system with the saturated actuator. Two neural networks were used as parametric structure to approximate the cost function and the corresponding control law, simulation results were given; an important issue to point out is that the neural network used in the algorithm implementation, increases the computational cost. Some robust controllers applied to UAVs have been reported in the specialized literature, for example, see References 15 and 16; in these works, only simulation results were reported. Moreover, the min max problem was addressed in Reference 17, an interesting approach was proposed for the infinite horizon nonlinear discrete optimal control problem. For the infinite horizon distributive cooperative optimal continuous problem for linear systems, one can cite Reference 18. Both in References 17 and 18 also report simulation results. Other interesting results on the nonlinear control for electromechanical systems have been recently reported in References 19-21, where continuous nonlinear controllers were proposed for robots manipulators and flexible structures based in the Lyapunov stability theory and neural networks approach.

Finally, in Reference 22, a infinite horizon discrete linear optimal control for altitude stabilization and takeoff phase was presented, experimental results and comparative study with a PD controller was addressed. According with the reported experimental results, the use of that discrete linear optimal control strategy reduces the energy consumption rate with respect to the PD controller.

Notice that, in the best knowledge of the authors, the most reported results in the literature present the optimal control design in continuous-time domain, and the most published papers have considered linear models to synthesize the optimal controllers. In the dynamic programming approach, the finite horizon optimal control problem for linear

systems in continuous domain involves the solution of a differential Riccati equation, which characterizes the Bellman function. Therefore, for the linear case, the problem has been fully solved. However, considering the same optimal control problem for nonlinear systems case, the lack of knowledge of the structure of Bellman function results in the fact that the synthesis of the optimal control is very complex. It is because the solution of the HJB equation results in a very hard task for the nonlinear case. If the continuous nonlinear optimal control of infinite horizon case is considered, the problem persists for the same reasons; similar problems are observed for the discrete nonlinear optimal control of infinite and finite horizon cases.

In this article, the finite horizon discrete nonlinear optimal control case is considered, with both final state and horizon fixed. This problem under some assumptions could be solved in a suboptimal sense. So, the main contributions are summarized as follows:

- A suboptimal nonlinear control sequence for discrete affine nonlinear systems and a quadratic performance index is backward founded step by step, proposing an approximation of the Bellman function, without solve the Bellman Equation. The founded suboptimal control sequence is given in an explicit way.
- The proposed suboptimal nonlinear control sequence can be explicitly compute for the case of a quadrotor, because it has an affine model. The penalty matrices are chosen in order to obtain different structures of the proposed suboptimal control.
- As in linear case, the penalty matrix associated with the controller restricts the magnitude of it.

However, it is important to mention that the convergence problem of the initial state to final state in certain numbers of steps (fixed final state and horizon) is even incipient.[23] However, it is important to emphasize that with our proposal the performance index decreases in each step.

Additionally, using an exact linearization, the discrete linear optimal control of finite horizon for a quadrotor is also synthesized. In order to contrast our proposal with a nonoptimized controller, a PD controller is used and tuned. An experimental comparative analysis gives evidence that the the discrete finite horizon optimal control strategy applied to a quadrotor represents a feasible option in order to improve the UAV performance.

The article is organized as follows: Section 1 shows an introduction of the issue dealt in this work and the previous published related papers. In Section 2, a discrete linear control of finite horizon is obtained by using a exact linearization and considering the quadrotor mathematical model expressed by three subsystems. The synthesis of a nonlinear suboptimal control which does not consider any linearization of the mathematical model is reported in Section 3. Next, Section 4describes the experimental platforms, while Section 5 deals with the experimental and simulation results using the proposed controllers and a PD controller. Finally, conclusions are given in Section 6.

2 | OPTIMAL LINEAR CONTROL OVER A FINITE HORIZON

The quadrotor scheme is presented in Figure 1 where the vector (x, y, z) denotes the position coordinates and (θ, ϕ, ψ) denotes the attitute pitch, roll, yaw angles, respectively. I is the inertial frame and B body frame.

Consider the following reduced model proposed in Reference 25:

$$\begin{aligned} m\ddot{x} &= -u\sin\theta \\ m\ddot{y} &= u\cos\theta\sin\phi \\ m\ddot{z} &= u\cos\theta\cos\phi - mg \\ \ddot{\phi} &= \tau_\phi \\ \ddot{\theta} &= \tau_\theta \\ \ddot{\psi} &= \tau_\psi, \end{aligned} \tag{1}$$

where $u, \tau_\phi, \tau_\theta$, and τ_ψ are the control inputs and $m = 1\ kg$ is the mass of the vehicle. In References 25 and 26 was exposed that an LQR could have some problems concerning to the region where it is valid, because it was obtained from a linear approximation of the dynamic model (1). In this article, the problem previously exposed has been solved by considering the mathematical model (1) as a set of three subsystems, which were obtained after to apply an exact linearization control

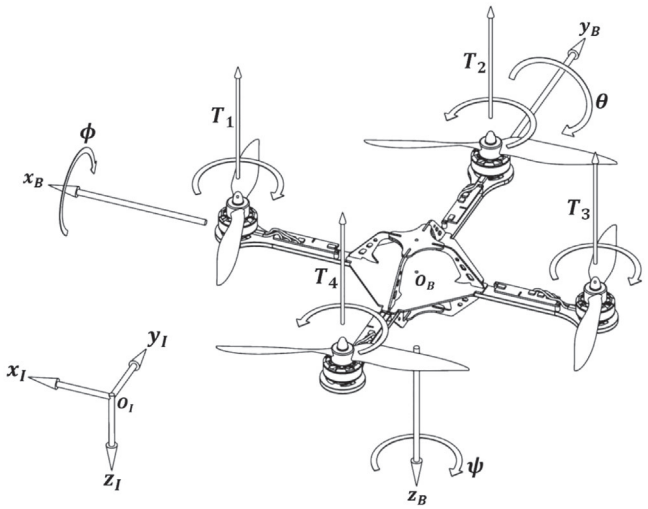

FIGURE 1 Coordinate frames in quadrotor (*Source:* Reference 24)

law. The simplified model given by the equation set (1) has been selected, in order to allow a simpler way to synthesize the controllers, considering that the experimental test are performed with a relative low velocity.[27,28] In References 29 and 30, the relevance of using simplified dynamic model has been shown by simulations and experimental tests. The first subsystem considered is the equation for the dynamic z.

In order to start with the controller synthesis, the basic definition about controllability for discrete systems is recalled.

Definition 1. The pair (x_o, x_1) is controllable if there exists an admissible control $\hat{u}(k)$ such that the system defined by $x(k+1) = f(x(k), \hat{u}(k))$ is transferred from x_0 to x_1 in N finite number of steps. Where $x(k), f(.,.) \in R^n$, $\hat{u}(k) \in R^m$.

An admissible control is considered as a bounded function. Note that one of the challenges for nonlinear discrete systems is to find the required number of steps N to achieve the convergence of the initial state x_0 to the final state x_1. In this work, the number of steps is considered fixed, consequently, this numbers of steps could be updated if the the final state x_1 in not reached with the fixed initial number of steps.

2.1 | Control for the subsystem z

First, consider the control of the subsystem z by an exact linearization of the model given in (1). To do this, consider the subsystem:

$$m\ddot{z} = u\cos\theta\cos\phi - mg,$$

considering $x_z = \begin{bmatrix} x_{1,z} & x_{2,z} \end{bmatrix}^T$, where $x_{1,z} = z$ and $x_{2,z} = \dot{z}$, and by the Euler approximation, follows that:

$$\begin{aligned} x_{1,z}(k+1) &= x_{1,z}(k) + Tx_{2,z}(k) \\ x_{2,z}(k+1) &= x_{2,z}(k) - Tg + T\left(\frac{\cos\theta(k)\cos\phi(k)}{m}\right)u(k), \end{aligned} \tag{2}$$

where T denotes the sampling time. Now, observe that the system (2) could be exactly linearized with the discrete control law:

$$u(k) = m(u_1(k) + g)(\cos\theta(k)\cos\phi(k))^{-1}, \tag{3}$$

with $\cos\theta(k)\cos\phi(k) \neq 0$, if $\theta, \phi \in \left(-\frac{\pi}{2}, \frac{\pi}{2}\right)$ which is a reasonable assumption according to operating conditions proposed for the quadrotor in this work. *Here $u_1(k)$ is a controller to determine*. Substituting the control law (3) into the subsystem (2), we arrive to:

$$x_z(k+1) = A_z x_z(k) + B_z u_1(k), \tag{4}$$

where $A_z = \begin{bmatrix} 1 & T \\ 0 & 1 \end{bmatrix}$, $B_z = \begin{bmatrix} 0 \\ T \end{bmatrix}$. It is not a hard task to verify that this pair is controllable in finite steps in the sense of Definition 1. Therefore, it seeks to find a control law applied to the system (4) minimizing the following performance index:

$$J_z = \frac{1}{2}\sum_{k=0}^{N_z-1}(x_z^T(k)Q_z x_z(k) + u_1^2(k)R_z) + \frac{1}{2}x_z^T(N_z)H_z x_z(N_z), \tag{5}$$

where $H_z, Q_z \geq 0, R_z > 0$ are given, here $N_z T = tf$ (horizon) with N_z integer. Then, we want to obtain a discrete control law $u_1(k)$, which minimizes J_z subject to (4). As it is very well known, the solution to this problem is given by:[31]

$$u_1^*(k) = -F_z(N_z - k)x_z^*(k), \quad \forall k = 0, \ldots, N_z - 1, \tag{6}$$

where

$$\begin{aligned} F_z(N_z - k) &= [R_z + B_z^T P_z(k-1)B_z]^{-1}B_z^T P_z(k-1)A_z, \\ P_z(k) &= [A_z + B_z F_z(N_z - k)]^T P_z(k-1)[A_z + B_z F_z(N_z - k)] \\ &\quad + F_z^T(N_z - k)RF_z(N_z - k) + Q_z, \quad \text{with } P_z(0) = H_z. \end{aligned}$$

This discrete control law generates an optimal trajectory for the system (4) and also minimizes the performance index (5).

2.2 | Subsystem ψ

Now, consider the yaw dynamic subsystem defined by:

$$\ddot{\psi} = \tau_\psi,$$

if $x_{1,\psi} = \psi$, and $x_{2,\psi} = \dot{\psi}$, the continuous model could be represented in the discrete time domain as:

$$x_\psi(k+1) = A_\psi x_\psi(k) + B_\psi \tau_\psi(k),$$

where $A_\psi = \begin{bmatrix} 1 & T \\ 0 & 1 \end{bmatrix}$, $B_\psi = \begin{bmatrix} 0 \\ T \end{bmatrix}$. Define a performance index as in (5), with H_ψ, $Q_\psi \geq 0$, and $R_\psi > 0$, and appropriate dimensions, the optimal control law is then given by

$$\tau_\psi^*(k) = -F_\psi(N_\psi - k)x_\psi^*(k), \forall k = 0, \ldots, N_\psi - 1,$$

where

$$\begin{aligned} F_\psi(N_\psi - k) &= [R_\psi + B_\psi^T P_\psi(k-1)B_\psi]^{-1}B_\psi^T P_\psi(k-1)A_\psi, \\ P_\psi(k) &= [A_\psi + B_\psi F_\psi(N_\psi - k)]^T P_\psi(k-1)[A_\psi + B_\psi F_\psi(N_\psi - k)] \\ &\quad + F_\psi^T(N_\psi - k)R_\psi F_\psi(N_\psi - k) + Q_\psi, \quad \text{with } P_\psi(0) = H_\psi. \end{aligned}$$

2.3 | Subsystem $y - \phi$

Consider the subsystem $y - \phi$ as:

$$\begin{aligned} m\ddot{y} &= u\cos\theta\sin\phi \\ \ddot{\phi} &= \tau_\phi, \end{aligned}$$

if $x_{1y} = y, x_{2y} = \dot{y}, x_{3\phi} = \phi, x_{4\phi} = \dot{\phi}$) and by using of Euler approximation, its discrete space state representation is given as follows

$$\begin{aligned} x_{1y}(k+1) &= x_{1y}(k) + Tx_{2y}(k) \\ x_{2y}(k+1) &= x_{2y}(k) + \frac{T}{m}u(k)\cos\theta(k)\sin x_{3\phi}(k) \\ x_{3\phi}(k+1) &= x_{3\phi}(k) + Tx_{4\phi}(k) \\ x_{4\phi}(k+1) &= T\tau_{\phi}(k) + x_{4\phi}(k), \end{aligned}$$

according with the definition for $u(k)$ given in (3), we have that second state in this subsystem is reduced to

$$x_{2y}(k+1) = T(u_1^*(k) + g)\tan x_{3\phi}(k) + x_{2y}(k).$$

However, according with the optimal control theory, $u_1^*(k)$ is equal to zero for $k = N_z T$. Then, for all $k \geq N_z T$, we arrive to:

$$x_{2y}(k+1) = gT\tan x_{3\phi}(k) + x_{2y}(k).$$

We want to find a control $\tau_{\phi}^*(k)$, such that $x_{y,\phi}(k) = \begin{bmatrix} x_{1y} & x_{2y} & x_{3\phi} & x_{4\phi} \end{bmatrix}^T$ goes to zero as fast as possible and the performance index

$$J_{y,\phi} = \frac{1}{2}\sum_{k=0}^{N_{\phi}-1}(x_{y,\phi}^T(k)Q_{y,\phi}x_{y,\phi}(k) + \tau_{\phi}^2(k)R_{\phi}) + \frac{1}{2}x_{y,\phi}^T(N_{\phi})H_{\phi}x_{\phi}(N_{\phi}), \tag{7}$$

is minimized, here $N_z < N_{\phi}$. If there exists an optimal control $\tau_{\phi}^*(k)$ which does this task, then $\tan(x_{3\phi}(k)) \approx x_{3\phi}(k)$ and we can design the optimal control $\tau_{\phi}^*(k)$ for the approximated system:

$$x_{y,\phi}(k+1) = A_{y,\phi}x_{y,\phi}(k) + B_{y,\phi}\tau_{\phi}(k),$$

where

$$A_{y,\phi} = \begin{bmatrix} 1 & T & 0 & 0 \\ 0 & 1 & gT & 0 \\ 0 & 0 & 1 & T \\ 0 & 0 & 0 & T \end{bmatrix}, \quad B_{y,\phi} = \begin{bmatrix} 0 \\ 0 \\ 0 \\ T \end{bmatrix}, \tag{8}$$

the pair $A_{y,\phi}, B_{y,\phi}$ is controllable in finite steps. Then, according with the optimal control theory, the control law $\tau_{\phi}^*(k)$ is defined as follows

$$\tau_{\phi}^*(k) = -F_{\phi}(N_{\phi} - k)x_{y,\phi}^*(k), \forall k = 0, \ldots, N_{\phi} - 1,$$

where

$$\begin{aligned} F_{\phi}(N_{\phi} - k) &= [R_{\phi} + B_{y,\phi}^T P_{\phi}(k-1)B_{y,\phi}]^{-1}B_{y,\phi}^T P_{\phi}(k-1)A_{y,\phi}, \\ P_{\phi}(k) &= [A_{y,\phi} + B_{y,\phi}F_{\phi}(N_{\phi} - k)]^T P_{\phi}(k-1)[A_{y,\phi} + B_{y,\phi}F_{\phi}(N_{\phi} - k)] \\ &\quad + F_{\phi}^T(N_{\phi} - k)R_{\phi}F_{\phi}(N_{\phi} - k) + Q_{\phi}, \quad \text{with } P_{\phi}(0) = H_{\phi}. \end{aligned}$$

Following a similar procedure, the optimal control law for the subsystem $x - \theta$ is synthesized.

2.4 | Subsystem $x - \theta$

Consider the subsystem $x - \theta$ defined as follows:

$$m\ddot{x} = -u \sin\theta$$
$$\ddot{\theta} = \tau_\theta,$$

its discrete state space representation ($x_{1x} = x, x_{2x} = \dot{x}, x_{3\theta} = \theta, x_{4\theta} = \dot{\theta}$) is given by

$$\begin{aligned} x_{1x}(k+1) &= x_{1x}(k) + Tx_{2x}(k), \\ x_{2x}(k+1) &= -\frac{T}{m}u(k)\sin x_{3\theta}(k) + x_{2x}(k), \\ x_{3\theta}(k+1) &= Tx_{4\theta}(k) + x_{3\theta}(k), \\ x_{4\theta}(k+1) &= T\tau_\theta(k) + x_{4\theta}(k). \end{aligned}$$

By similar arguments previously applied, the optimal control law $\tau_\theta^*(k)$ which minimizes a quadratic criterion similar to given by (7) is:

$$\tau_\theta^*(k) = -F_\theta(N_\theta - k)x_{x,\theta}^*(k), \forall k = 0, \ldots, N_\theta - 1,$$

where

$$\begin{aligned} F_\theta(N_\theta - k) &= [R_\theta + B_{x,\theta}^T P_\theta(k-1)B_{x,\theta}]^{-1} B_{x,\theta}^T P_\theta(k-1)A_{x,\theta}, \\ P_\theta(k) &= [A_{x,\theta} + B_{x,\theta}F_\theta(N_\theta - k)]^T P_\theta(k-1)[A_{x,\theta} + B_{x,\theta}F_\theta(N_\theta - k)] \\ &\quad + F_\theta^T(N_\theta - k)R_\theta F_\theta(N_\theta - k) + Q_\theta, \quad \text{with } P_\theta(0) = H_\theta. \end{aligned}$$

The design of all those controllers is based on the main idea that the subsystems are linear (using exact linearization or assumptions about the angles of the orientation, then the controllability is verified in the local sense). Theoretically, the synthesized controllers could be applied without restrictions on the initial conditions and set points, however under the assumptions which allowed to obtain linear models, in the practice it is not so. In order to validate this, we made an experimental study later. In the next section, we propose to use dynamic programming in discrete domain. Using the fact that the mathematical model of the quadrotor is affine, see Reference 32, we obtain an optimal nonlinear control sequence which minimizes a finite horizon discrete performance index.

3 | OPTIMIZATION PROCEDURE OF FINITE HORIZON

3.1 | Suboptimal discrete nonlinear control for affine systems

Consider the nonlinear discrete affine system as follows

$$\bar{x}(k+1) = f_0(\bar{x}(k)) + f_1(\bar{x}(k))\bar{u}(k), \tag{9}$$

where $k = 0,1, \ldots, N, \bar{x}(k), f_0(\bar{x}(k)) \in R^n, f_1(\bar{x}(k)) \in R^{n\times m}$ and $\bar{u}(k) \in R^m$. Defining now the following performance index

$$J = \frac{1}{2}\bar{x}^T(N)H\bar{x}(N) + \frac{1}{2}\sum_{k=0}^{N-1}\{\bar{x}^T(k)Q\bar{x}(k) + \bar{u}^T(k)R\bar{u}(k)\}, \tag{10}$$

where $Q \geq 0$ and $R > 0$ are matrices of appropriate dimensions and $t_f = TN$ is the horizon, with T defining the sample period. Assume that the pair of points (x_0, x_{t_f}) of the system (9) satisfy Definition 1. The essence of the following dynamic programming approach in discrete time was proposed originally in Reference 31, and here it is modified to obtain an

approximation of the optimal sequence. First, define the following notation:

$$J^*_{N,N} = \frac{1}{2}\bar{x}^T(N)H\bar{x}(N).$$

Note that this term does not depend of the control law $\bar{u}(N)$, and it could be called the optimal value of J in the discrete time N. Then, the next step is defined as follows

$$\begin{aligned} J^*_{N-1,N} &= \min_{\bar{u}(N-1)} \left\{ \frac{1}{2}\bar{x}^T(N)H\bar{x}(N) + \frac{1}{2}\bar{x}^T(N-1)Q\bar{x}(N-1) + \frac{1}{2}\bar{u}^T(N-1)R\bar{u}(N-1) \right\} \\ &= \min_{\bar{u}(N-1)} \left\{ J^*_{N,N} + \frac{1}{2}\bar{x}^T(N-1)Q\bar{x}(N-1) + \frac{1}{2}\bar{u}^T(N-1)R\bar{u}(N-1) \right\}. \end{aligned}$$

The value of the state $\bar{x}(N)$ can be obtained from state space equation given by (9), then:

$$\begin{aligned} J^*_{N-1,N}(\bar{x}(N-1),\bar{u}(N-1)) = \min_{\bar{u}(N-1)} \Big\{ & \frac{1}{2}[f_0(\bar{x}(N-1)) + f_1(\bar{x}(N-1))\bar{u}(N-1)]^T H \\ & \times [f_0(\bar{x}(N-1)) + f_1(\bar{x}(N-1))\bar{u}(N-1)] \\ & + \left(\frac{1}{2}\bar{x}^T(N-1)Q\bar{x}(N-1) + \frac{1}{2}\bar{u}^T(N-1)R\bar{u}(N-1) \right) \Big\}, \end{aligned} \tag{11}$$

in this step, we proceed in the traditional way in order to find the minimal value of $J_{N-1,N}$. It follows that

$$\bar{u}^*(N-1) = -[f_1^T(\bar{x}(N-1))Hf_1(\bar{x}(N-1)) + R]^{-1} f_1^T(\bar{x}(N-1))Hf_0(\bar{x}(N-1)), \tag{12}$$

the positive definiteness of the matrix R guarantees that $[f_1^T(\bar{x}(N-1))Hf_1(\bar{x}(N-1)) + R]^{-1}$ exists. Observe that the control given by (12) is the optimal control in local sense, because

$$\frac{\partial^2 J_{N-1,N}(\bar{x}(N-1),\bar{u}(N-1))}{\partial^2 \bar{u}(N-1)} = R > 0. \tag{13}$$

The existence of a minimum is guaranteed, because the right side in Equation (11) is strongly convex with respect to $\bar{u}(N-1)$. For the following step $N-2$, note that the value of $\bar{u}^*(N-1)$ is the optimal value in the step $N-1$, and according with the Bellman optimality principle, this control generates the optimal value for $\bar{x}(N-1)$. Then for $N-2$ step, we have that:

$$\begin{aligned} J^*_{N-2,N}(\bar{x}(N-2),\bar{u}(N-1),\bar{u}(N-2)) = \min_{\bar{u}(N-1),\bar{u}(N-2)} \Big\{ & \frac{1}{2}\bar{x}(N)^T H\bar{x}(N) + \frac{1}{2}\bar{x}^T(N-1)Q\bar{x}(N-1) \\ & + \left(\frac{1}{2}\bar{x}^T(N-2)Q\bar{x}(N-2) + \frac{1}{2}\bar{u}^T(N-1)R\bar{u}(N-1) \right) \\ & + \left(\frac{1}{2}\bar{u}^T(N-2)R\bar{u}(N-2) \right) \Big\}. \end{aligned} \tag{14}$$

Note that the term which involves $\bar{x}(N)$, depends on the control $\bar{u}(N-1)$ and the term with $\bar{x}(N-2)$ depends of the control $\bar{u}(N-3)$, only the term with $\bar{x}(N-1)$ depends of the control $\bar{u}(N-2)$. But, the control $\bar{u}(N-1)$ found in the previous step is optimal and $\bar{x}(N-1)$ is given by the state equation (9), it follows that

$$\begin{aligned} J^*_{N-2,N}(\bar{x}(N-2),\bar{u}(N-2)) = \min_{\bar{u}(N-2)} \Big\{ & \frac{1}{2}\bar{x}(N)^T H\bar{x}(N) + \frac{1}{2}[f_0(\bar{x}(N-2)) + f_1(\bar{x}(N-2))\bar{u}(N-2)]^T Q \\ & \times [f_0(\bar{x}(N-2)) + f_1(\bar{x}(N-2))\bar{u}(N-2)] \\ & + \left(\frac{1}{2}\bar{x}^T(N-2)Q\bar{x}(N-2) + \frac{1}{2}\bar{u}^T(N-1)R\bar{u}(N-1) \right) + \left(\frac{1}{2}\bar{u}^T(N-2)R\bar{u}(N-2) \right) \Big\}. \end{aligned} \tag{15}$$

In order to avoid the solution of type Riccati equation in discrete domain which is a very complex problem, Equation (15) is used to obtain the suboptimal control $\bar{u}^*(N-2)$. Similar to the previous case, note that the equation given by (15) is strongly convex with respect to $\bar{u}(N-2)$ and this fact guarantees the existence of a minimum. However,

$\overline{u}^*(N-2)$ is only an approximation to the optimal value of $\overline{u}(N-2)$, because as it is very well know the optimal control signal $\overline{u}(N-2)$ should be found by applying the solution of the type Riccati equation for the nonlinear discrete case, being a not easy task. Acting in the usual way in order to find the suboptimal control $\overline{u}^*(N-2)$, we get

$$\overline{u}^*(N-2) = -[f_1^T(\overline{x}(N-2))Qf_1(\overline{x}(N-1)) + R]^{-1} f_1^T(\overline{x}(N-1))Qf_0(\overline{x}(N-1)).$$

It is not a hard task to extend the previous results and set up the general equations as follows

$$J^*_{N-k,N}(\overline{x}(N-k), \overline{u}(N-k)) = J^*_{N-k+1,N} + \frac{1}{2}\{\overline{x}^T(N-k)Q\overline{x}(N-k) + \overline{u}^T(N-k)R\overline{u}(N-k)\},$$
$$\overline{u}^*(N-k) = -[f_1^T(\overline{x}(N-k))Qf_1(\overline{x}(N-k)) + R]^{-1} f_1^T(\overline{x}(N-k))Qf_0(\overline{x}(N-k)),$$
$$\text{for all } k = 2, \ldots, N.$$

This suboptimal sequence here obtained guarantees that an approximation for the minimal value of the performance index (10) is reached, see Equation (13). In the next section, this suboptimal discrete scheme is applied on the quadrotor platform.

3.2 | Quadrotor suboptimally controlled

This section is devoted to show the application of the previously exposed approach on a quadrotor helicopter. The discrete dynamic model used in this work for the controller synthesis is deducted from a reduced continuous mathematical model of this aerial platform, which was presented in Reference 26. The synthesis of the finite horizon discrete suboptimal nonlinear control based on dynamic programming approach was already exposed above, and only will be applied on this discrete representation. The complete system is divided in three subsystems, as was proposed in Reference 26. However, in contrast to other approaches,[12,22] we obtain the four suboptimal controllers without use exact linearization or quasilinear approximations of the model.

3.2.1 | Control for the subsystem $z - \psi$

Consider the dynamics for z and ψ:

$$m\ddot{z}(t) = u\cos\theta(t)\cos\phi(t) - mg$$
$$\ddot{\psi}(t) = \tau_\psi.$$

Let $x_{1,z} = z$, $x_{2,z} = \dot{z}$, $x_{1,\psi} = \psi$, $x_{2,\psi} = \dot{\psi}$ be , then the state space representation is defined by:

$$\dot{x}_{z,\psi} = f_{0,z,\psi}(x_{z,\psi}) + f_{1,z,\psi}(\theta, \phi)u_z,$$

where $x_{z,\psi} = [x_{1,z}\ x_{2,z}\ x_{1,\psi}\ x_{2,\psi}]^T$, $u_z = [u\ \tau_\psi]^T$, and

$$f_{0,z,\psi}(x_{z,\psi}) = \begin{bmatrix} x_{2,z} \\ -mg \\ x_{2,\psi} \\ 0 \end{bmatrix}, \quad f_{1,z,\psi}(\theta, \phi) = \begin{bmatrix} 0 & 0 \\ \cos\theta\cos\phi & 0 \\ 0 & 0 \\ 0 & 1 \end{bmatrix}.$$

As the design of the control scheme is carried out in discrete domain, consider the following equivalent discrete system obtained by the Euler approximation:

$$x_{z,\psi}(k+1) = f_{0,z\psi}(x_{z,\psi}(k)) + f_{1,z\psi}(\theta(k), \phi(k))u_z(k), \tag{16}$$

with

$$f_{0,z\psi}(x_{z,\psi}(k)) = \begin{bmatrix} x_{2,z}(k)T_s + x_{1,z}(k) \\ x_{2,z}(k) - gT_s \\ x_{2,\psi}(k)T_s + x_{1,\psi}(k) \\ x_{2,\psi}(k) \end{bmatrix}, \quad f_{1,z\psi}(k) = \begin{bmatrix} 0 & 0 \\ \frac{T_s}{m}\cos(\theta(k))\cos(\phi(k)) & 0 \\ 0 & 0 \\ 0 & T_s \end{bmatrix},$$

where T_s represents the sample period. The aim is to obtain the control vector $u_z(k)$ such that the performance index

$$J_{z,\psi} = \frac{1}{2}x_{z,\psi}^T(N_1)H_0x_{z,\psi}(N_1) + \frac{1}{2}\sum_{k=0}^{N_1-1}\{x_{z,\psi}^T(k)Q_{z,\psi}x_{z,\psi} + u_z^T(k)R_{z,\psi}u_z(k)\}, \tag{17}$$

$$H_0,\ \ Q_{z,\psi} \in R^{4\times4},\ \ R_{z,\psi} \in R^{2\times2},\ \ H_0,\ \ Q_{z,\psi} \geq 0,\ \ R_{z,\psi} > 0, \tag{18}$$

is minimized subject to (16), here $t_f = N_1T_s$, for some integer N_1. According with the considerations exposed above, the suboptimal control u_z^* has the following structure:

$$u_z^*(N_1-k) = \begin{cases} -[f_{1,z\psi}^T(N_1-k)H_0f_{1,z\psi}(N_1-k) + R_{z,\psi}]^{-1}f_{1,z\psi}^T(N_1-k)H_0f_{0,z\psi}(x_{z,\psi}(k)), & \text{for } k=1, \\ -[f_{1,z\psi}^T(N_1-k)Q_{z,\psi}f_{1,z\psi}(N_1-k) + R_{z,\psi}]^{-1}f_{1,z\psi}^T(N_1-k)Q_{z,\psi}f_{0,z\psi}(x_{z,\psi}(k)), & \text{for all } k>1, \end{cases} \tag{19}$$

The control law (19) assumes that the variables $\theta(k)$, $\phi(k)$ are appropriated controlled in the interval $[t_0, t_f]$ (they are addressed in the subsystems $x-\theta$ and $y-\phi$, respectively, and later exposed). Under this assumption, the vector $f_{1,z\psi}^T(N_1-k)$ is bounded, allowing to conclude that $u_z^*(N_1-k)$ is an admissible control law. Substituting the vectors $f_{1,z\psi}^T(N_1-k)$, $f_{0,z\psi}(x_{z,\psi}(k))$ and the matrices $Q_{z,\psi}$ and $R_{z,\psi}$, it is possible to find an explicit form of the suboptimal control $u_z^*(N_1-k)$. For this purpose, consider the matrices H_0 and $Q_{z,\psi}$ as follows:

$$H_0 = \begin{bmatrix} h_{0,11} & h_{0,12} & 0 & 0 \\ h_{0,21} & h_{0,22} & 0 & 0 \\ 0 & 0 & h_{0,33} & h_{0,34} \\ 0 & 0 & h_{0,43} & h_{0,44} \end{bmatrix}, Q_{z,\psi} = \begin{bmatrix} q_{z\psi,11} & q_{z\psi,12} & 0 & 0 \\ q_{z\psi,21} & q_{z\psi,22} & 0 & 0 \\ 0 & 0 & q_{z\psi,33} & q_{z\psi,34} \\ 0 & 0 & q_{z\psi,43} & q_{z\psi,44} \end{bmatrix},$$

which are positive semidefinite matrices with adequate entries. After direct calculations, the optimal controllers $u(N_1-k)$ and $\tau_\psi(N_1-k)$ given by (19) are:

$$u^*(N_1-k) = -F_1(N_1-k)\begin{bmatrix} x_{1,z}(N_1-k) \\ x_{2,z}(N_1-k) \end{bmatrix} + F_2(N_1-k),$$

$$\tau_\psi^*(N_1-k) = -G_1\begin{bmatrix} x_{1,\psi}(N_1-k) \\ x_{2,\psi}(N_1-k) \end{bmatrix},$$

where

$$F_1(N_1-k) = \left[\frac{mT_s\cos(\theta(N_1-k))\cos(\phi(N_1-k))}{r_{11}m^2 + E_{22}T_s^2\cos^2\theta(N_1-k)\cos^2\phi(N_1-k)}\right]\begin{bmatrix} E_{21} & (E_{21}T_s + E_{22}) \end{bmatrix},$$

$$F_2(N_1-k) = \left[\frac{mT_s\cos(\theta(N_1-k))\cos(\phi(N_1-k))}{r_{11}m^2 + E_{22}T_s^2\cos^2\theta(N_1-k)\cos^2\phi(N_1-k)}\right]E_{22}gT_s,$$

$$G_1 = \left(\frac{T_s}{E_{44}T_s^2 + r_{22}}\right)\begin{bmatrix} E_{43} & (E_{43}T_s + E_{44}) \end{bmatrix},$$

and

$$E_{ij} = \begin{cases} h_{ij}, & \text{for } k = 1, \\ q_{ij}, & \text{for } k > 1. \end{cases}$$

It is clear that both controllers are linear with respect to state $x_{z,\psi}$. Notice that a particular selection of the matrices H_0 and $Q_{z,\psi}$ produces particular structures for these controllers.

3.2.2 | Subsystem $y - \phi$

Consider now the subsystem $y - \phi$:

$$\begin{aligned} m\ddot{y} &= u\cos\theta\sin\phi \\ \ddot{\phi} &= \tau_\phi. \end{aligned}$$

The space state representation can be obtained as follows ($x_{1y} = y$, $x_{2y} = \dot{y}$, $x_{1,\phi} = \phi$, $x_{2\phi} = \dot{\phi}$):

$$\begin{aligned} \dot{x}_{1y} &= x_{2y} \\ \dot{x}_{2y} &= u\cos\theta\sin(x_{1,\phi}) \\ \dot{x}_{1\phi} &= x_{2,\phi} \\ \dot{x}_{2\phi} &= \tau_\phi. \end{aligned}$$

Then, its corresponding discrete approximation is given by:

$$\begin{aligned} x_{1y}(k+1) &= T_s x_{2y}(k) + x_{1y}(k) \\ x_{2y}(k+1) &= T_s u(k)\cos(\theta(k))\sin(x_{1,\phi}(k)) + x_{2y}(k) \\ x_{1\phi}(k+1) &= T_s x_{2\phi}(k) + x_{1\phi}(k) \\ x_{2\phi}(k+1) &= T_s \tau_\phi(k) + x_{2\phi}(k). \end{aligned}$$

Substituting the control $u(k)$ by $u_z^*(k)$ obtained in the previous section, we arrive to:

$$x_{y,\phi}(k+1) = f_0(x_{y,\phi}(k), u_z^*(k)) + f_1\tau_\phi(k), \tag{20}$$

where

$$f_0(x_{y,\phi}(k), u_z^*(k)) = \begin{bmatrix} T_s x_{2y}(k) + x_{1y}(k) \\ T_s u_z^*(k)\cos(\theta(k))\sin(x_{1,\phi}(k)) + x_{2y}(k) \\ T_s x_{2\phi}(k) + x_{1\phi}(k) \\ x_{2\phi}(k) \end{bmatrix}, f_1 = \begin{bmatrix} 0 \\ 0 \\ 0 \\ T_s \end{bmatrix},$$

we want to find the control τ_ϕ such that the performance index

$$\begin{aligned} J_{y,\phi} &= \frac{1}{2}x_{y,\phi}^T(N_2)H_1 x_{y,\phi}(N) + \frac{1}{2}\sum_{k=0}^{N_2-1}\{x_{y,\phi}^T(k)Q_{y,\phi}x_{y,\phi} + \tau_\phi^2(k)R_\phi\}, \\ Q_{y,\phi} &\in R^{4\times 4}, \quad R_\phi \in R, \quad Q_{y,\phi} \geq 0, \quad R_\phi > 0, \end{aligned}$$

subject to (20) is minimized. According with the above exposed, we have that

$$\tau_\phi^*(N_2 - k) = [f_1^T E_{y,\phi} f_1 + R_\phi]^{-1} f_1^T E_{y,\phi} f_0(x_{y,\phi}^*(N_2 - k), u_z^*(N_2 - k)),$$

where

$$E_{y,\phi}(i,j) = \begin{cases} h_{1,ij}, & \text{for } k = 1, \\ q_{y\phi,ij}, & \text{for } k > 1. \end{cases}$$

Defining the matrix $E_{y,\phi}$ as follows:

$$E_{y,\phi} = \begin{bmatrix} e_{11} & 0 & 0 & e_{14} \\ 0 & e_{22} & 0 & 0 \\ 0 & 0 & e_{33} & e_{34} \\ e_{41} & 0 & e_{43} & e_{44} \end{bmatrix},$$

we have that

$$f_1^T Q_{y,\phi} f_1 + R_\phi = \begin{bmatrix} 0 \\ 0 \\ 0 \\ T_s \end{bmatrix}^T \begin{bmatrix} e_{11} & 0 & 0 & e_{14} \\ 0 & e_{22} & 0 & 0 \\ 0 & 0 & e_{33} & e_{34} \\ e_{41} & 0 & e_{43} & e_{44} \end{bmatrix} \times \begin{bmatrix} 0 \\ 0 \\ 0 \\ T_s \end{bmatrix} + R_\phi = e_{44} t_s^2 + R_\phi$$

and

$$\begin{aligned} f_1^T Q_{y,\phi} f_0(x_{y,\phi}(N-k), u_z^*(N-k)) = & \begin{bmatrix} 0 \\ 0 \\ 0 \\ T_s \end{bmatrix}^T \begin{bmatrix} e_{11} & 0 & 0 & e_{14} \\ 0 & e_{22} & 0 & 0 \\ 0 & 0 & e_{33} & e_{34} \\ e_{41} & 0 & e_{43} & e_{44} \end{bmatrix} \\ & \times \begin{bmatrix} T_s x_{2y}(N-k) + x_{1,y}(N-k) \\ T_s u_z^*(N-k)\cos(\theta(N-k))\sin(\phi(N-k)) + x_{2y}(N-k) \\ T_s x_{2,\phi}(N-k) + x_{1,\phi}(N-k) \\ x_{2,\phi}(N-k) \end{bmatrix} \\ = & e_{43} T_s x_{1,\phi}(N-k) + (e_{43} T_s^2 + e_{44} T_s) x_{2\phi}(N-k) + e_{41} T_s x_{1,y}(N-k) + e_{41} T_s^2 x_{2,y}(N-k), \end{aligned}$$

it follows that:

$$\tau_\phi^*(N-k) = -F_\phi x_{y,\phi}^*(N-k),$$

where

$$F_\phi = \frac{1}{e_{44} T_s^2 + R_\phi} \begin{bmatrix} e_{41} T_s & e_{41} T_s^2 & e_{43} T_s & e_{44} T_s + e_{43} T_s^2 \end{bmatrix}.$$

The selected matrices $Q_{y,\phi}$ and H give a linear optimal controller τ_ϕ^*. Similar steps will be made to synthesize the control law τ_θ^* in the following section.

3.2.3 | Subsystem $x - \theta$

Dynamic model related with this subsystem is given by:

$$\begin{aligned} m\ddot{x} &= -u \sin\theta \\ \ddot{\theta} &= \tau_\theta, \end{aligned}$$

considering the state variables $x_{1,x} = x$, $x_{2,x} = \dot{x}$, $x_{1,\theta} = \theta$,and $x_{2,\theta} = \dot{\theta}$, its state representation is defined as follows:

$$\begin{aligned}\dot{x}_{1,x} &= x_{2,x}\\ \dot{x}_{2,x} &= -u\sin(x_{1,\theta})\\ \dot{x}_{1,\theta} &= x_{2,\theta}\\ \dot{x}_{2,\theta} &= \tau_\theta\end{aligned}$$

and the corresponding discrete domain representation is expressed by:

$$\begin{aligned}x_{1,x}(k+1) &= T_s x_{2,x}(k) + x_{1,x}(k)\\ x_{2,x}(k+1) &= -T_s u(k)\sin(x_{1,\theta}(k)) + x_{2,x}(k)\\ x_{1,\theta}(k+1) &= T_s x_{2,\theta}(k) + x_{1,\theta}(k)\\ x_{2,\theta}(k+1) &= T_s \tau_\theta(k) + x_{2,\theta}(k).\end{aligned}$$

Substituting the control $u(k)$ by $u_z^*(k)$ it follows that:

$$x_{x,\theta}(k+1) = \bar{f}_0(x_{x,\theta}(k), u_z^*(k)) + f_1\tau_\theta(k),$$

where

$$\bar{f}_0(x_{x,\theta}(k), u_z^*(k)) = \begin{bmatrix} T_s x_{2,x}(k) + x_{1,x}(k)\\ -T_s u_z^*(k)\sin(x_{1,\theta}(k)) + x_{2,x}(k)\\ T_s x_{2,\theta}(k) + x_{1,\theta}(k)\\ x_{2,\theta}(k)\end{bmatrix}, \quad f_1 = \begin{bmatrix}0\\0\\0\\T_s\end{bmatrix},$$

we want to find the control law τ_θ^*, such that the performance index

$$\begin{aligned}J_{x,\theta} &= \frac{1}{2}x_{x,\theta}^T(N_3)H_2x_{x,\theta}(N_3) + \frac{1}{2}\sum_{k=0}^{N-1}\{x_{x,\theta}^T(k)Q_{x,\theta}x_{x,\theta} + \tau_\theta^2(k)R_\theta\},\\ Q_{x,\theta} &\in R^{4\times4},\ \ R_\theta \in R,\ \ Q_{x,\theta} \geq 0,\ \ R_\theta > 0,\end{aligned}$$

is minimized. Then

$$\tau_\theta^*(N_3 - k) = -[f_1^T Q_{x,\theta} f_1 + R_\theta]^{-1} f_1^T E_{x,\theta}\bar{f}_0(x_{x,\theta}^*(N_3 - k), u_z^*(N_3 - k)).$$

As previously, consider a matrix $E_{x,\theta}$ with the following structure:

$$E_{x,\theta} = \begin{bmatrix}\tilde{e}_{11} & 0 & 0 & \tilde{e}_{14}\\ 0 & \tilde{e}_{22} & 0 & 0\\ 0 & 0 & \tilde{e}_{33} & \tilde{e}_{43}\\ \tilde{e}_{41} & 0 & \tilde{e}_{43} & \tilde{e}_{44}\end{bmatrix}, \quad E_{y,\phi}(i,j) = \begin{cases} h_{2,ij}, & \text{for } k = 1,\\ q_{x,\theta,ij}, & \text{for } k > 1.\end{cases}$$

then, we get

$$\begin{aligned}f_1^T Q_{x,\theta} f_1 + R_\theta &= \begin{bmatrix}0\\0\\0\\T_s\end{bmatrix}^T\begin{bmatrix}\tilde{e}_{11} & 0 & 0 & \tilde{e}_{14}\\ 0 & \tilde{e}_{22} & 0 & 0\\ 0 & 0 & \tilde{e}_{33} & \tilde{e}_{34}\\ \tilde{e}_{41} & 0 & \tilde{e}_{43} & \tilde{e}_{44}\end{bmatrix}\begin{bmatrix}0\\0\\0\\T_s\end{bmatrix} + R_\theta\\ &= \tilde{e}_{44}t_s^2 + R_\theta\end{aligned}$$

and

$$f_1^T Q_{x,\theta} \bar{f}_0(x_{x,\theta}(N-k), u_z^*(N-k)) = \begin{bmatrix} 0 \\ 0 \\ 0 \\ T_s \end{bmatrix}^T \begin{bmatrix} \tilde{e}_{11} & 0 & 0 & \tilde{e}_{14} \\ 0 & \tilde{e}_{22} & 0 & 0 \\ 0 & 0 & \tilde{e}_{33} & \tilde{e}_{34} \\ \tilde{e}_{41} & 0 & \tilde{e}_{43} & \tilde{e}_{44} \end{bmatrix} \times \begin{bmatrix} T_s x_{2,x}(N-k) + x_{1,x}(N-k) \\ T_s u^* \cos(\theta(N-k)) \sin(x_{1,\phi}(N-k)) + x_{2,x}(N-k) \\ T_s x_{2,\theta}(N-k) + x_{1,\theta}(N-k) \\ x_{2,\theta}(N-k) \end{bmatrix}$$
$$= T_s \tilde{e}_{43} x_{1,\theta}(N-k) + (T_s \tilde{e}_{44} + T_s^2 \tilde{e}_{43}) x_{2,\theta}(N-k) + T_s \tilde{e}_{41} x_{1,x}(N-k) + T_s^2 \tilde{e}_{41} x_{2,x}(N-k),$$

it follows that:

$$\tau_\theta^*(N-k) = -F_\theta x_{x,\theta}^*(N-k),$$

where

$$F_\theta = \frac{1}{\tilde{e}_{44} t_s^2 + R_\theta} \begin{bmatrix} T_s \tilde{e}_{41} & T_s^2 \tilde{e}_{41} & T_s \tilde{e}_{43} & T_s \tilde{e}_{44} + T_s^2 \tilde{e}_{43} \end{bmatrix}.$$

Notice that, with an appropriated structure and selection of the matrices Q and H for each one of performance indexes corresponding to a specific subsystem, the control laws τ_θ^*, τ_ϕ^*, and τ_ψ^* are linear. Then, we have chosen this option in order to obtain simpler controllers. In addition, the selection of the penalization matrices plays another important role in the resulting controllers structures, this fact will be shown in next section.

4 | EXPERIMENTAL PLATFORMS

Two experimental platforms were used to test the performance of the controllers under study. Following, these platforms are described.

4.1 | 4-DOF experimental platform

The dynamics of a real flying quad-rotor has 6 degrees-of-freedom (DOF) movement, three for angular orientation and three more for position. The first experimental platform used allows angular movement in roll and pitch angles (ϕ and θ) and displacements along x and z axes, see Figure 2. The coordinated control of all four rotors will provide the desired altitude z, while the x movement is produced by changing $(f_1 + f_4)$ - $(f_2 + f_3)$. The pitch torque is also produced by the force relationship recently described. Finally, the roll torque is produced by the difference $(f_1 + f_2)$-$(f_3 + f_4)$. Therefore, currently testbed allows only 4 DOF in 3D space. According to this setup platform, we can obtain a similar result as a real quadrotor aircraft evolving inside of a limited space. Quadrotor is fixing with two metal bars which avoid the movements in yaw angle ψ and displacements along y axis. Two joints and pistons at the top of quad-rotor allow angular movements around the x and y axes in order to produced until 15° and 60° in roll and pitch angles, respectively.

This educational platform has autopilot based on RabbitCore module RCM4300 (8-Bit Flash memory program). The discrete time optimal control laws to stabilize the mini helicopter running at 200 Hz. The mini-core has the following main features: operates at 58.98 Mhz (10-ns Cycle Time), with 512K bits serial I2C EEPROM memory, low-power (1.8-V Core, 3.3-V I/O), 4 PWM channels (10-bit resolution), 8 ADC channels (12-bit resolution), 5 serial ports, 2 input-capture channels, 10 timers (16-bit resolution) and I2C port. Also this microcontroller manages the inertial measurements provided by the IMU module. The IMU module is based on Inertial Navigation System by Microstrain, it measures angular

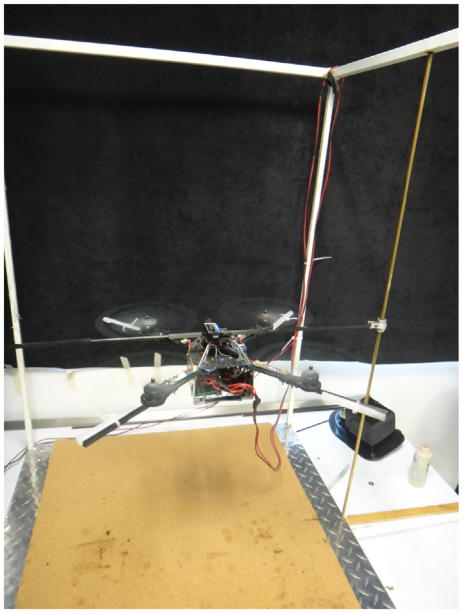

FIGURE 2 Quadrotor experimental setup of 4DOF [Colour figure can be viewed at wileyonlinelibrary.com]

rates $(\dot{\phi}, \dot{\theta}, \dot{\psi})$ and three angular positions (ϕ, θ, ψ). Moreover this experimental setup has external communication using RS232 protocol, then it can send and receive data from a external PC, where complex control algorithm could be programmed and tested in real-time. The communication device used to have available this feature in our platform is Xbee Modem working at 2.4GHz and 115 200 bauds per second in order to avoid additional delays in the control loop. Matlab Simulink interface was developed using serial communication tools for send/receive control, attitude, and position signals through the computer and experimental platform. Ultrasonic sensor with resolution of 4 cm is used to estimate the z position and Euler approximation for the z velocity. For safety reasons, we use radio-control communication and the autopilot detects when the quad-rotor is experienced high translational and angular velocities and when it arrives to z position limits in order to avoid crashes.

4.2 | 6-DOF experimental platform

The second experimental platform is described now. The platform, which was used for outdoor testing, was built on the frame "Turnigy Talon Quadcopter (V2.0)" made of carbon fiber and 550mm wide. In this chassis has been mounted an autopilot "Pixhawk" by 3D Robotics, this autopilot is based on a 32-bit ARM Cortex M4 core with FPU processor running at 168Mhz with 256 Kb of RAM and 2MB of Flash memory. The Pixhawk has internally an inertial build in unit, composed by two accelerometers, two magnetometers of 14-bit resolution, a 16-bit gyroscope and a MS5611-01ba barometer with resolution of 10 cm. This autopilot has 5 UART serial ports, 3 inputs for RF receiver, Spektrum DSM, Futaba S.BUS, and PPM Sum Signal, besides it has a port 12c, SPI, 2 CAN ports and two ADC ports (see Figure 3). The data transmission

FIGURE 3 Quadrotor experimental setup of 6DOF [Colour figure can be viewed at wileyonlinelibrary.com]

during the experiments was performed via serial telemetry devices by 3D Robotics which work at a frequency of 915 MHz, the data were received through a graphical interface in Matlab performed in real time. The batteries used for flights were of Lithium Polymer (LiPo) 3-cell 2800 mA. Figure 3 shows the experimental platform.

In both platforms, the suboptimal nonlinear controller, the optimal linear controller, and the PD controller were tested. The obtained experimental results are described below.

5 | EXPERIMENTAL AND SIMULATIONS RESULTS

5.1 | 4-DOF experimental platform

Experimental tests were performed and their results are presented in this section. Using the first considered platform (restricted for the angles ϕ and θ and x and y axes), three controllers have been tested for regulate the altitude z. Those are: linear optimal and nonlinear suboptimal controllers with finite horizon and the PD controller. For the finite horizon linear optimal control, we choose the following penalization matrices

$$Q_z = \begin{bmatrix} 0.56 & 0 \\ 0 & 8 \end{bmatrix}, \quad H_z = \begin{bmatrix} 3 & 0 \\ 0 & 4.5 \end{bmatrix}, \quad R_z = 375, \tag{21}$$

which are used in the performance index (5). These penalty matrices were adjusted via simulations and experimental validation, until a satisfactory plant performance was obtained. The following matrices are chosen to be applied in the performance indexes (17-18), when the nonlinear suboptimal control (19) is considered.

$$H_0 = \begin{bmatrix} 1.5 & 0.5 & 0 & 0 \\ 0.5 & 2.25 & 0 & 0 \\ 0 & 0 & 1.5 & 0.5 \\ 0 & 0 & 0.5 & 2.25 \end{bmatrix}, \quad Q_{z,\psi} = \begin{bmatrix} 18 & 10.1 & 0 & 0 \\ 10.1 & 8.6 & 0 & 0 \\ 0 & 0 & 5 & 3 \\ 0 & 0 & 3 & 5 \end{bmatrix}, \quad R_{z,\psi} = diag\{0.81, 0.81\}. \tag{22}$$

The last penalty matrices were chosen as in the linear case. The objective of these tests is to validate the feasibility of the proposed control laws, which consider the energy consumption and the convergence to the Set Point. For both cases when the optimal controllers (linear and nonlinear) are applied, the sampling rate was stated at 10 ms and the horizon at 40 seconds, after of this time a PD controller is used, and this controller was tuned using the method exposed in Reference 22, which is based on two specific time parameters: overshot and settling time. A routine of takeoff for the vehicle is defined, in this profile the last set point was defined as 30 cm and the predefined ramp reaches this altitude at 15 seconds. Figure 4A shows the response of the system in altitude when the nonlinear suboptimal control is used. Figure 4B displays the control signal when the control law given by (19) is applied.

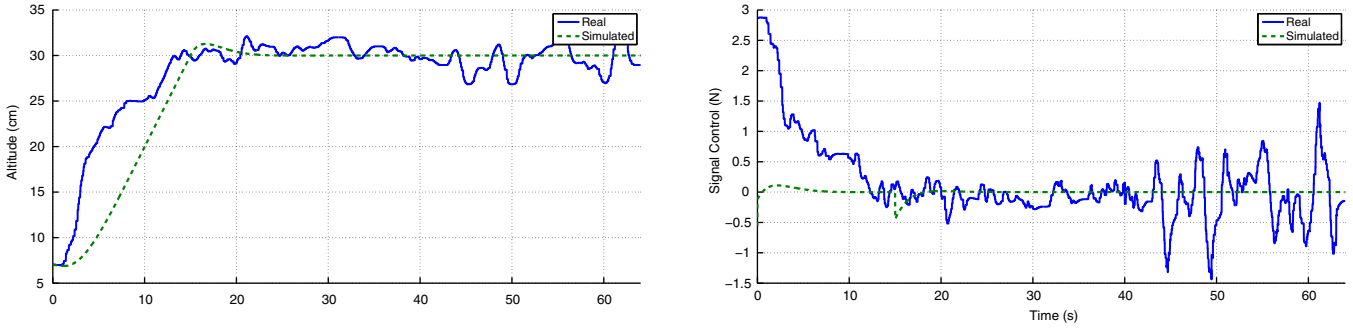

(A) Altitude of the vehicle

(B) Control signal

FIGURE 4 Stabilization in z using the nonlinear suboptimal discrete control law and control signal applied [Colour figure can be viewed at wileyonlinelibrary.com]

Figure 5A displays the altitude behavior when it is driven by a PD controller. Moreover, Figure 5displays the control signal produced by the PD controller. Notice that for the 4-DOF experimental platform, disturbances produced by the own vehicle propellers are present, due to the fact that the altitude Set Point was fixed to low altitude (30 cm), representing by itself an experimental robustness test for the considered controllers.

Figure 6A shows the altitude stabilization when the linear optimal control with finite horizon is considered, while Figure 6B displays the control signal of the linear optimal control of finite horizon with exact linearization.

The deviations in the experiments could be explained by the fact that the accuracy of the altitude sensor is about 3 to 4 cm, which represents an uncertainty in this measure. For instance, the sensor is located on the aerial platform at a distance of 5 cm from the ground (nearby to the minimum measurement of the sensor). Then, when the helicopter is landed, this sensor reports zero altitude or another measure around of 5 cm.

A graphic summary of response of the three applied controller (suboptimal nonlinear, optimal linear, and PD) can be seen in Figure 7.

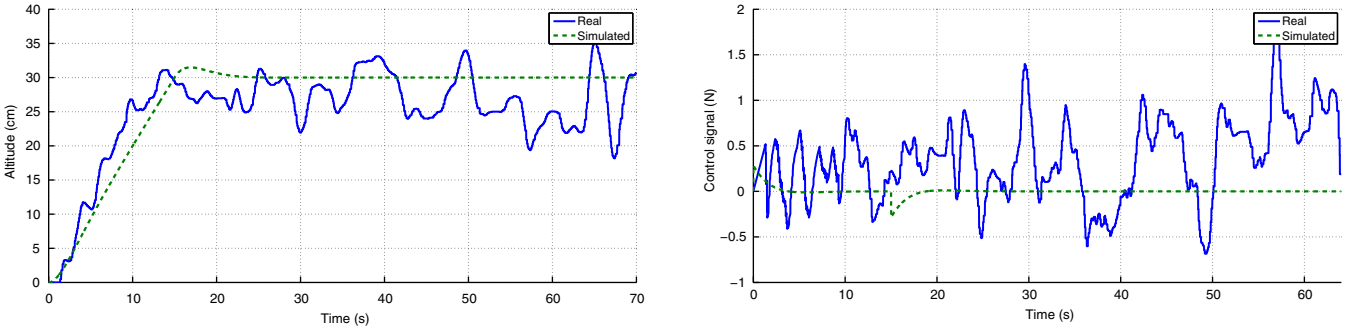

(A) Altitude of the vehicle (B) Control signal

FIGURE 5 Stabilization in z using a PD controller and control signal applied [Colour figure can be viewed at wileyonlinelibrary.com]

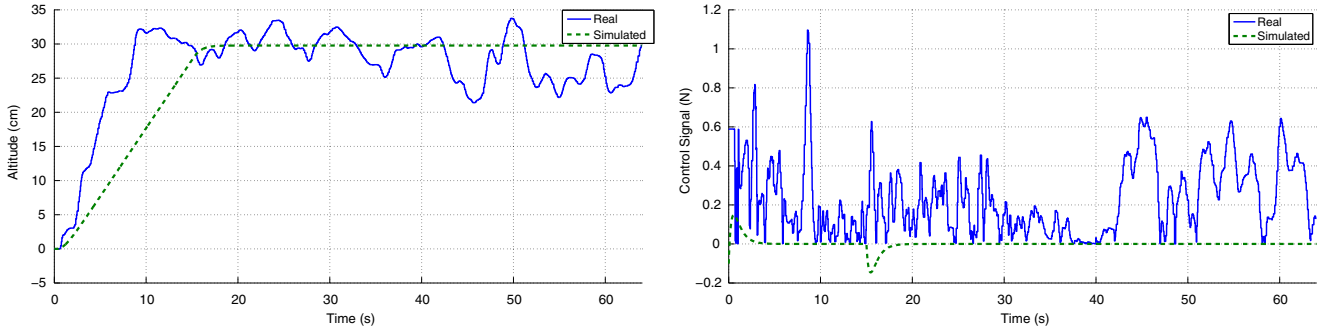

(A) Altitude of the vehicle (B) Control signal

FIGURE 6 Altitude stabilization of the vehicle using optimal linear control with exact linearization and control signal applied [Colour figure can be viewed at wileyonlinelibrary.com]

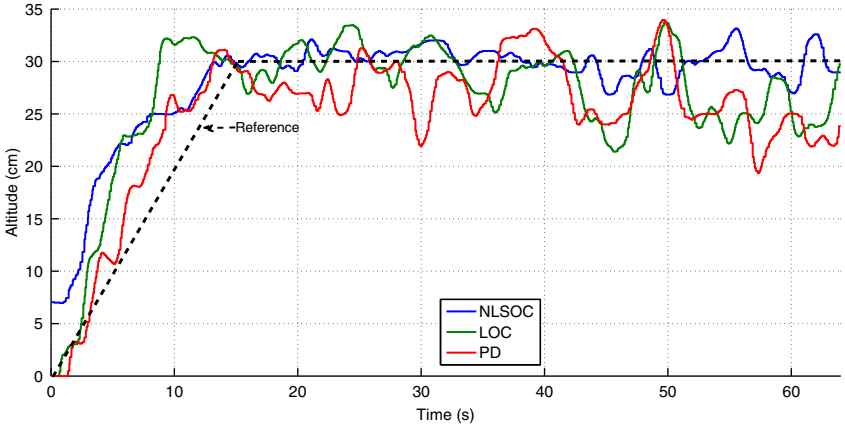

FIGURE 7 Comparative of the responses of the three considered controllers [Colour figure can be viewed at wileyonlinelibrary.com]

TABLE 1 Comparative of performance and saving energy: Experimental and Simulation test

Performance Index	$NLSOC_{exp}$	LOC_{exp}	PD_{exp}	$NLSOC_{simul}$	LOC_{simul}	PD_{simul}
J_z given by (5) and (18)	15 214.236	490.791	—	11 860.4	560.89	—
J_u	1732.648	757.023	1396.423	1221.5	692.4	1121
J_e	16 108.471	20 675.477	28 089.648	23 869	26 869	24 365

The performance and saving energy issues are summarized and compared in Table 1. In order to compute the energy saving index, we have defined the following quadratic index $J_u = \sum(abs(u(k)))$, while to evaluate and quantify the UAV performance, we have used the index $J_e = \sum(\|e(k)\|)$ based on error signals, where the error vector is defined by $e(k) = [30cm \quad 0] - [z \quad \dot{z}_d]$, with $\dot{z}_d$ denoting the discrete version $\dot{z}$.

Here, *NLOC*, *LOC*, and *PID* denote nonlinear suboptimal control, linear optimal control, and proportional integral derivative control, respectively, and the subscripts *"exp"* and *"simul"* indicate the experimental and simulation results. The difference on these numeric performances index values could be explained to a great extent by the uncertainty related with the altitude sensor and to a lesser extent by the nonmodeled dynamics. However, the same trend can be observed in the experimental and simulation tests. Penalization matrices for both optimal controllers are given by (21) and (22). Observe that similar performances are obtained for the linear optimal control with exact linearization and the PD controller, but the linear optimal control has a smaller energy consumption rate. According with the altitude error, the performance of the nonlinear optimal control is better than the others controllers but using more energy. Performing the real-time experiments, the mathematical model, the easiness to adjust the parameters control, and the robustness of the control scheme have been validated. In this sense, notice that the parameters control of the linear and nonlinear optimized controllers, depend of the penalty matrices, and for the both cases (linear and nonlinear optimized controllers), the selection was made using a previous digital simulation, with this, the choice was simplest.

5.2 | 6-DOF experimental platform

Outdoor experiments are made in order to test the proposed controllers in more complicated situations, and in this case, the four inputs for the quadrotor (u, τ_θ, τ_ϕ, and τ_ψ) are considered. The three controllers under study were developed in order to generate the previous name four inputs. Two task are considered: The stabilization in altitude and a trajectory tracking routine.

5.2.1 | Altitude control task

With respect to the altitude stabilization using the optimal linear controller of finite horizon, the following penalization matrices were used in the performance indexes (5) and the associated index with the subsystem ψ:

$$\begin{aligned} Q_{z,\psi} &= diag\{9\times10^4, 6\times10^4, 1.6\times10^6, 1\times10^6\}, \\ R_{z,\psi} &= diag\{32, 28\}, \\ H_{z,\psi} &= diag\{100{,}150, 100{,}150\}. \end{aligned} \tag{23}$$

The optimal linear controllers τ_ϕ and τ_θ minimizing their respective quadratic performance indexes of type given in (7), use the following penalization matrices:

$$\begin{aligned} Q_{y,\phi} = Q_{x,\theta} &= diag\{1\times10^4, 9\times10^4, 1\times10^6, 1.80\times10^5\}, \\ R_\phi = R_\theta &= 20, \\ H_\phi = H_\theta &= diag\{70, 32, 30, 30\}, \end{aligned} \tag{24}$$

and for τ_ψ it was used same penalization matrices. As in indoor environment tests, the choosing of these penalty matrices was made via a previous digital simulation.

The horizon was stated at 10 minutes with sampling period of 10 ms. After this time the vehicle is manually descended. As in 4-DOF platform, a routine of takeoff for the vehicle is given in outdoor environment, in this profile the last Set Point was defined at 2 m. The experiment was made 10 times in order to give more evidence in our conclusions about the feasibility of the proposed control strategies and the collected data. It is important to remark that wind cross was present during the experiments. Figure 8A,B displays the response of the vehicle and the applied control signal, respectively.

As it was mentioned above, the accuracy of the altitude sensor is 3 or 4 cm, it causes the oscillations in the variable z, besides that, cross wind was presented during the tests, affecting the performance of the plant. The apparent chattering in the control signal is only the time scale, when a zoom is applied in all control signals, it is possible to verify that the control signals has low frequency.

Following with the set of test, for the nonlinear discrete suboptimal control described in Section 3, the following penalization matrices were considered to implement this controller:

$$
\begin{aligned}
H_0 &= \begin{bmatrix} 4200 & 3800 & 0 & 0 \\ 3800 & 4300 & 0 & 0 \\ 0 & 0 & 17\,500 & 16\,000 \\ 0 & 0 & 16\,000 & 17\,500 \end{bmatrix}, \quad Q_{z,\psi} = \begin{bmatrix} 4000 & 3900 & 0 & 0 \\ 3900 & 4000 & 0 & 0 \\ 0 & 0 & 17\,500 & 17\,000 \\ 0 & 0 & 17\,000 & 17\,500 \end{bmatrix}, \\
R_{z,\psi} &= diag\{0.47, 0.5\}, \\
Q_{x,\theta} &= Q_{y,\phi} = \begin{bmatrix} 8\times10^5 & 0 & 0 & 129 \\ 0 & 8\times10^5 & 0 & 8000 \\ 0 & 0 & 8500 & 8450 \\ 129 & 8000 & 8450 & 8500 \end{bmatrix}, \\
H_{0,x} &= H_{0,y} = \begin{bmatrix} 8\times10^5 & 0 & 0 & 129 \\ 0 & 8\times10^5 & 0 & 5000 \\ 0 & 0 & 8500 & 8450 \\ 129 & 5000 & 8450 & 8500 \end{bmatrix}, \\
R_\phi &= R_\theta = 0.45,
\end{aligned} \tag{25}
$$

all these matrices were obtained using a digital simulation routine and after implementing in the obtained controllers acting on the experimental platform. Figure 9A,B displays the behavior of the vehicle and the applied control signal.

A new, in these experiments, wind cross was present and its explains the overshot and oscillations in the variable z. That is why we conducted 10 experiments with same controller to conclude the efficiency of controller. By last, a PD controller heuristically tuned was considered with the following gains:

$$
\begin{aligned}
&K_{p,z} = 42, K_{d,z} = 35, \quad K_{p,\psi} = 100, K_{d,\psi} = 86, \\
&K_{p,x} = K_{p,y} = 31, \quad K_{d,x} = K_{d,y} = 32, \\
&K_{p,\theta} = K_{p,\phi} = 170, \quad K_{d,\theta} = K_{d,\phi} = 63.
\end{aligned} \tag{26}
$$

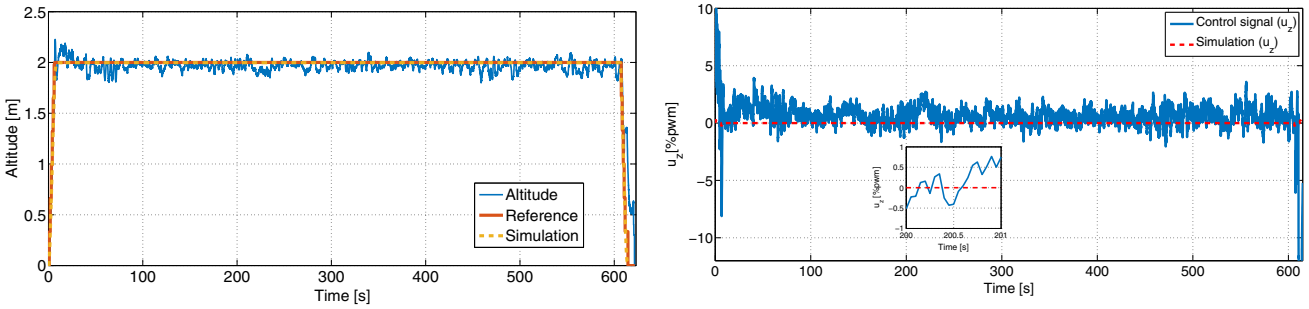

(A) Altitude of the vehicle

(B) Control signal

FIGURE 8 Altitude stabilization of the vehicle using optimal linear control with exact linearization and control signal applied with Set Point of 2 m, for outdoor flight [Colour figure can be viewed at wileyonlinelibrary.com]

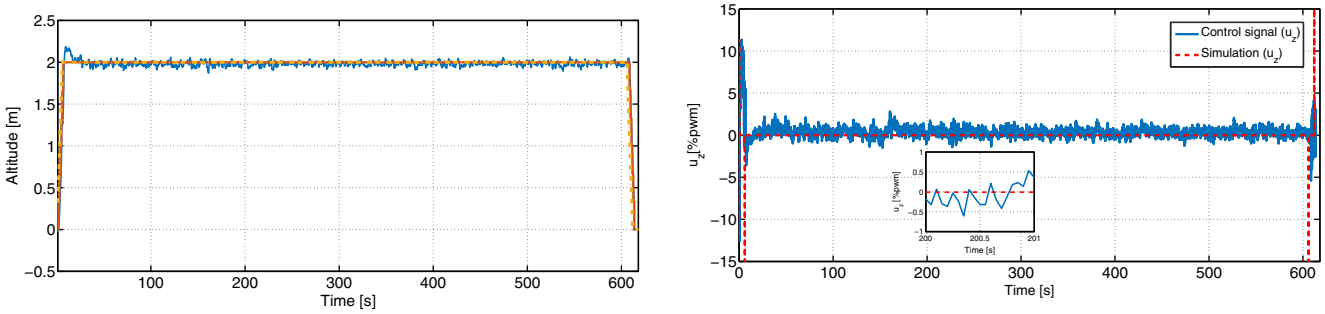

(A) Altitude of the vehicle (B) Control signal

FIGURE 9 Altitude stabilization of the vehicle using the suboptimal nonlinear control and control signal applied with Set Point of 2 m, for outdoor flight [Colour figure can be viewed at wileyonlinelibrary.com]

Figure 10A,B displays the response of the vehicle and the applied control signal when PD controllers were used.

The overshot induced by the PD controller is lower than that produced by the nonlinear suboptimal and linear controllers; however, its performance is poorer than the performances obtained by the other two optimal controllers. The objective to include experiments considering PD controllers, it is to contrast optimized versus nonoptimized controllers. This contrast between controllers is shown in Table 2, which displays the data mean for the 10 experiments made with each controller versus the simulation results.

According with the results presented in Table 2, notice that when all inputs in the quadrotor are considered, lower amount of the energy is used by the optimal linear control, followed by the suboptimal nonlinear control and finally the PD controller. However, the suboptimal nonlinear control presents a smaller error than the others two controllers. It could be explained with the fact that the suboptimal nonlinear control takes into account a more extended mathematical model of the vehicle (the controller has a relative complex structure), while the optimal linear control is synthesized from a linear model of the vehicle and has a simpler structure. Finally, the PD controller has a similar structure of the optimal linear control, but with no optimization, having a higher energy consumption and poorer performance. Furthermore, for each one of the tested controllers (with 10 corresponding experiments), theirs standard deviations of error means are and they are presented in Table 3.

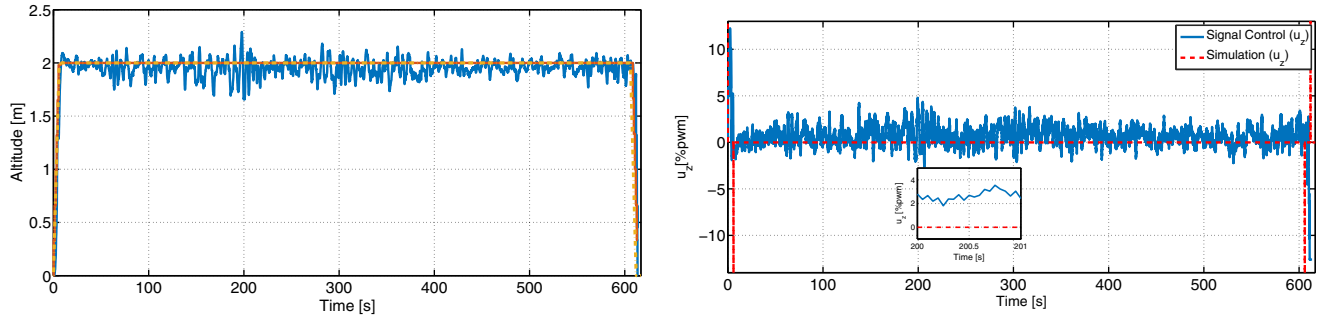

(A) Altitude of the vehicle (B) Control signal

FIGURE 10 Altitude stabilization of the vehicle using PD controllers and control signal applied with Set Point of 2 m, for outdoor flight [Colour figure can be viewed at wileyonlinelibrary.com]

TABLE 2 Comparative of performance and saving energy: Experimental and Simulation test, for outdoor flight

Performance Index	$NLSOC_{exp}$	LOC_{exp}	PD_{exp}	$NLSOC_{simul}$	LOC_{simul}	PD_{simul}
J_z given by (5)	1.35×10^7	4.47×10^8	—	1.28×10^7	3.79×10^8	—
$J_{u,\tau_\phi,\tau_\psi,\tau_\theta}$	8967.7	8818.3	11 553.57	5268	1181.80	6304
J_e	738.31	914.3	1090	184	253	236

TABLE 3 Comparative of error standard deviation: Experimental and Simulation test, for outdoor flight

	$NLSOC_{exp}$	LOC_{exp}	PD_{exp}
Error Mean	0.18 m	0.19 m	0.21 m
Standard deviation	0.05	0.06	0.08

From Table 3, it is clear that the error means for the three controllers are similar and all them have small values of error standard deviations, but the suboptimal nonlinear controller presents lower dispersion around 0.18 m, and according with Table 2 with lower energy consumption.

5.2.2 | Trajectory tracking task

Now, experimental and simulation results are presented when the Set Point in $x-y$ describes a circle with a 1 m radius and the Set Point in z is 1.5 m. The set points for the orientation variables (θ, ϕ, ψ), angular and translational velocities $(\dot{\theta}, \dot{\phi}, \dot{\psi}, \dot{x}, \dot{y}, \dot{z})$ were all adjusted to zero. First, consider the optimal linear control with same penalization matrices given in (23), these matrices were used in the performance indexes (5) and the performance index associated with the variable ψ. For the optimal linear controllers τ_ϕ and τ_θ, the penalization matrices used are given by (24). The horizon was chosen as 60 seconds and the sampling rate was 10 ms, the takeoff, trajectory tracking, and landing are part to the full task. As previously, the experiment was made 10 times in order to give more evidence in our conclusions about it, and also wind cross was present in the tests. Figures 11 and 12 display the UAV behavior during this task and the applied control signal.

The deviations of the UAV with respect to the reference could be explained by external disturbances, despite the presence of them, an acceptable performance could be observed. Figure 12 displays the real control signal versus the simulation. As in the simulation does not exist disturbances, we can observe a small control signal, however, the real control

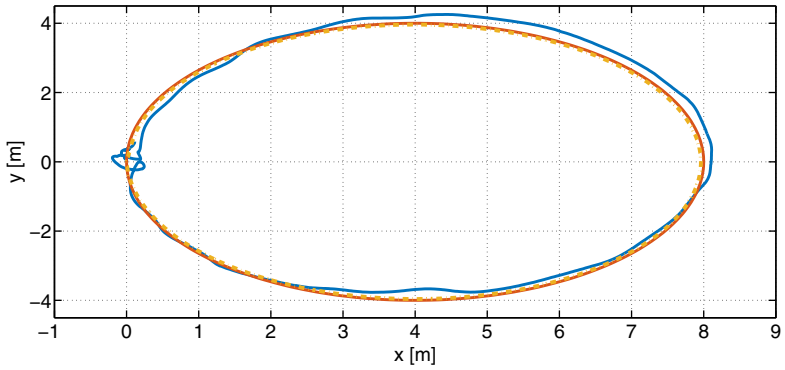

FIGURE 11 Position of the vehicle using optimal linear control with exact linearization with a trajectory tracking task, for outdoor flight [Colour figure can be viewed at wileyonlinelibrary.com]

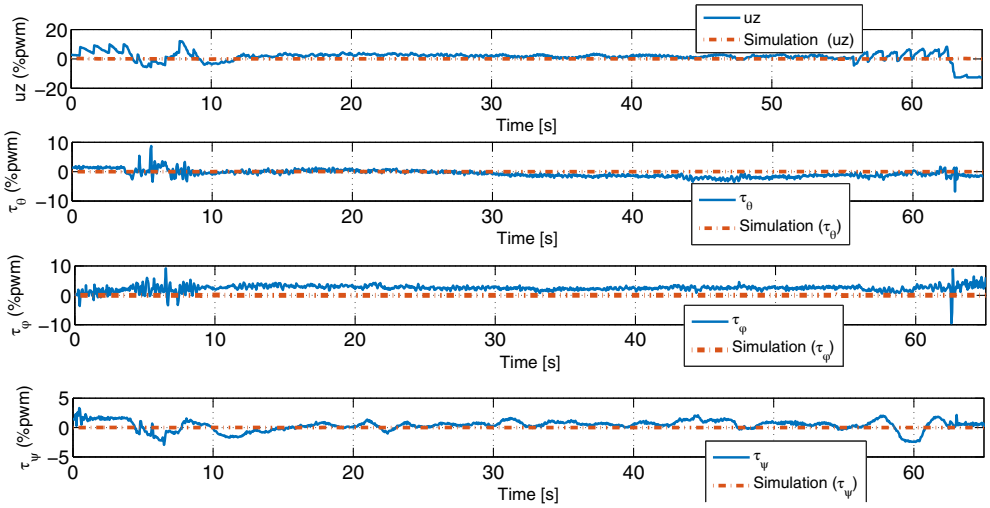

FIGURE 12 Control signal for the optimal linear control with exact linearization with a trajectory tracking task, for outdoor flight [Colour figure can be viewed at wileyonlinelibrary.com]

signal is relative small too. Figure 13A,B displays the position in the axes x, y, and z and the orientation of the vehicle when the optimal linear control is used. Similar responses could be observed when the experimental and simulation results are compared.

Figure 14A,B displays the velocities for the variables x, y, and z and the orientation of the vehicle when a optimal linear control is used.

For the suboptimal nonlinear controller, Figures 15 and 16 show the response of the vehicle and the applied control signal.

Although external disturbances are present, could observe a good tracking in the response on the plant. Figure 17A,B shows the position in the axis x, y, and z and the orientation of the quadrotor for the suboptimal nonlinear control is used. In these figures, experimental and simulation results are compared, and similar responses could be seen.

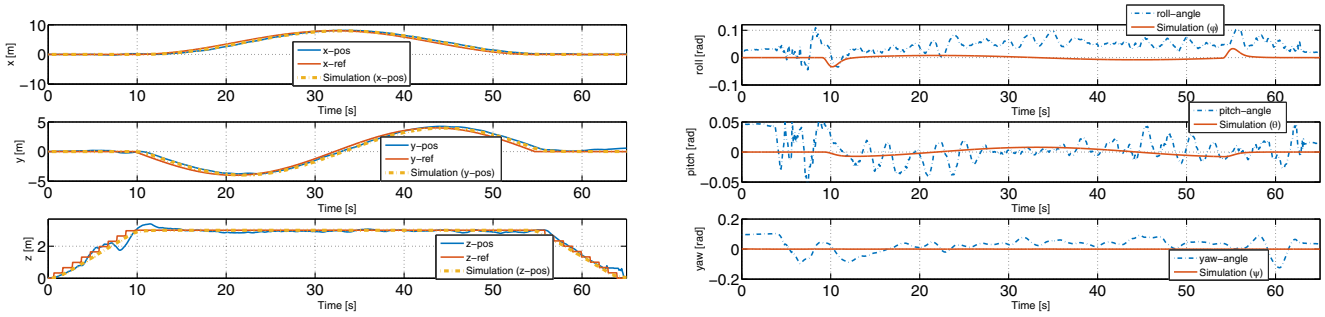

(A) Position of the vehicle

(B) Orientation of the vehicle

FIGURE 13 Position and orientation of the vehicle using the optimal linear control in a trajectory tracking task for outdoor flight [Colour figure can be viewed at wileyonlinelibrary.com]

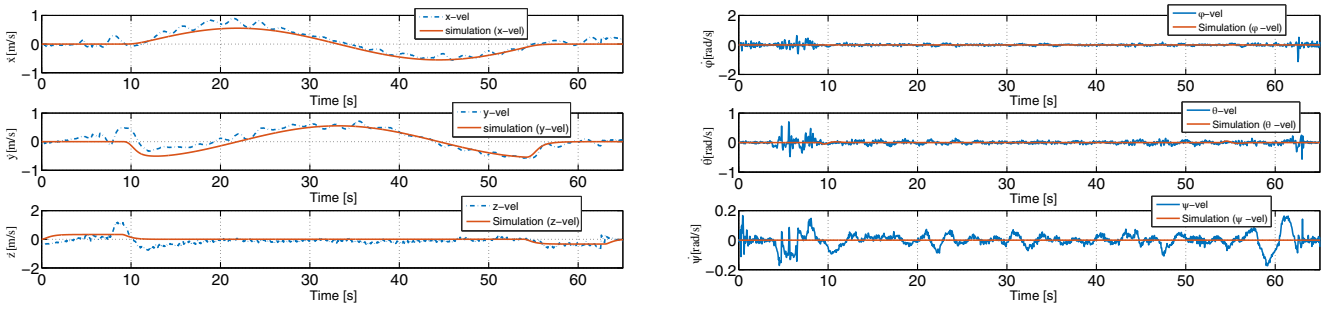

(A) Velocities of the vehicle

(B) Angular velocities of the vehicle

FIGURE 14 Velocities of the vehicle using the optimal linear control in a trajectory tracking task for outdoor flight [Colour figure can be viewed at wileyonlinelibrary.com]

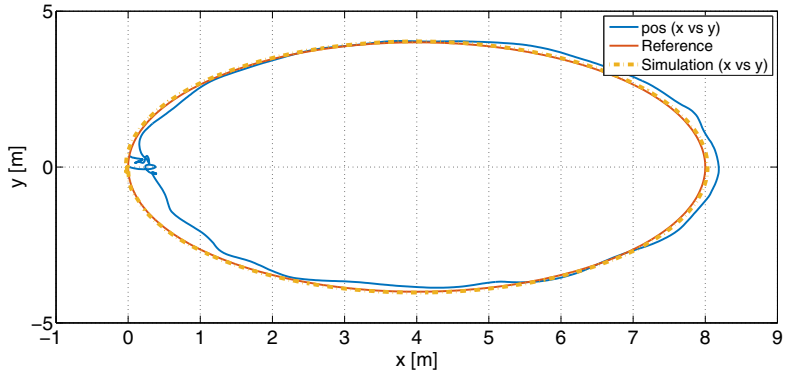

FIGURE 15 Position of the vehicle using suboptimal nonlinear control with a trajectory tracking task, for outdoor flight [Colour figure can be viewed at wileyonlinelibrary.com]

FIGURE 16 Control signal for the suboptimal nonlinear control with a trajectory tracking task, for outdoor flight [Colour figure can be viewed at wileyonlinelibrary.com]

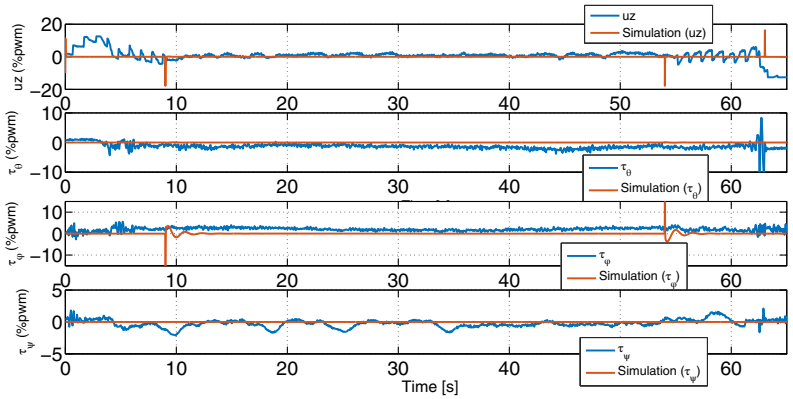

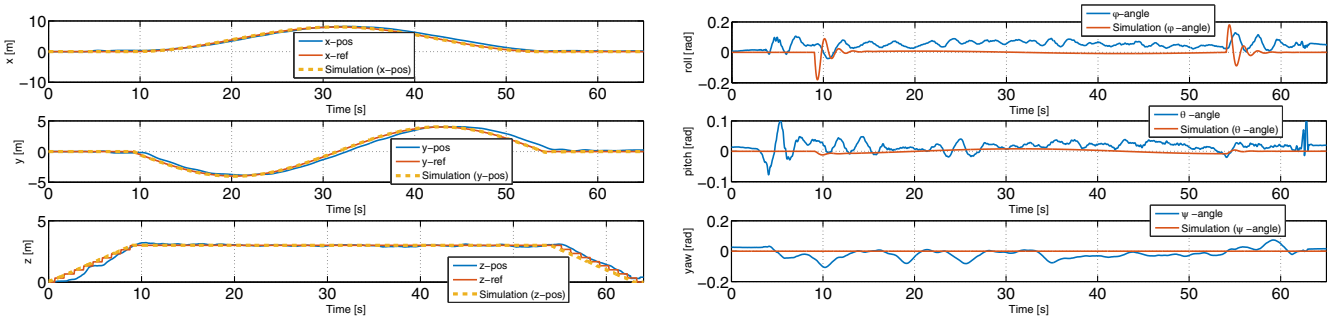

(A) Position of the vehicle

(B) Orientation of the vehicle

FIGURE 17 Position and orientation of the vehicle using the suboptimal nonlinear control in a trajectory tracking task for outdoor flight [Colour figure can be viewed at wileyonlinelibrary.com]

Figure 18A,B displays the velocities for the variables x, y, and z and the orientation of the vehicle when the suboptimal nonlinear control is used.

By last, the experimental and simulation results using PD controllers are presented. In Figures 19 and 20can be seen the response of the vehicle and the applied control signal when PD controllers are used.

Even though for this presented experiments there was external disturbances acting on the UAV, in order to conclude the efficiency of the three controllers, the experiments were made 10 times. In this way, in the comparison analysis, the external disturbances effects could be better handled because in some experiments there was less disturbances than others, and the mean of them were considered to compute the performance indexes. Figure 21A,B show the position in the axes x, y, and z and the orientation of the quadrotor when PD controllers were used. As the previous results, similar experimental and simulation results could be observed.

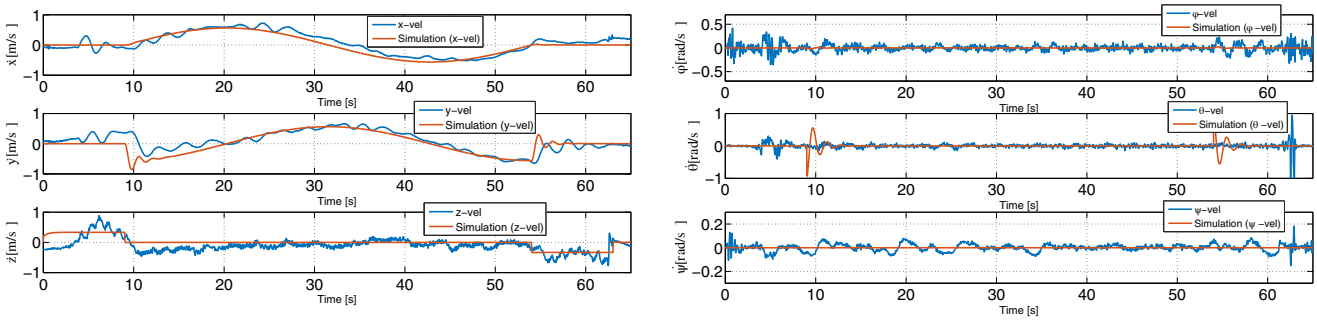

(A) Velocities of the vehicle

(B) Angular velocities of the vehicle

FIGURE 18 Velocities of the vehicle using the suboptimal nonlinear control in a trajectory tracking task for outdoor flight [Colour figure can be viewed at wileyonlinelibrary.com]

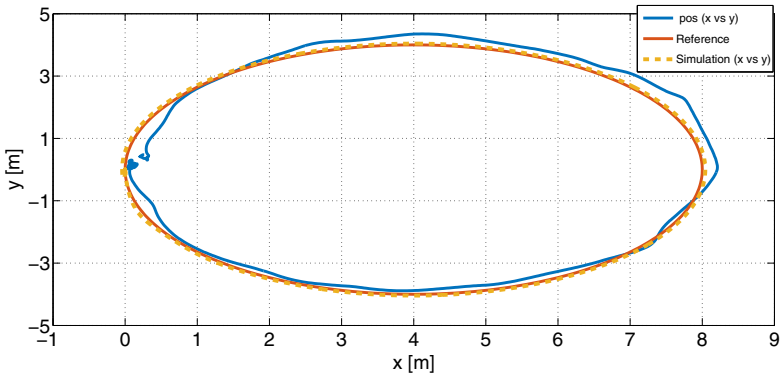

FIGURE 19 Position of the vehicle using PD controllers with a trajectory tracking task, for outdoor flight [Colour figure can be viewed at wileyonlinelibrary.com]

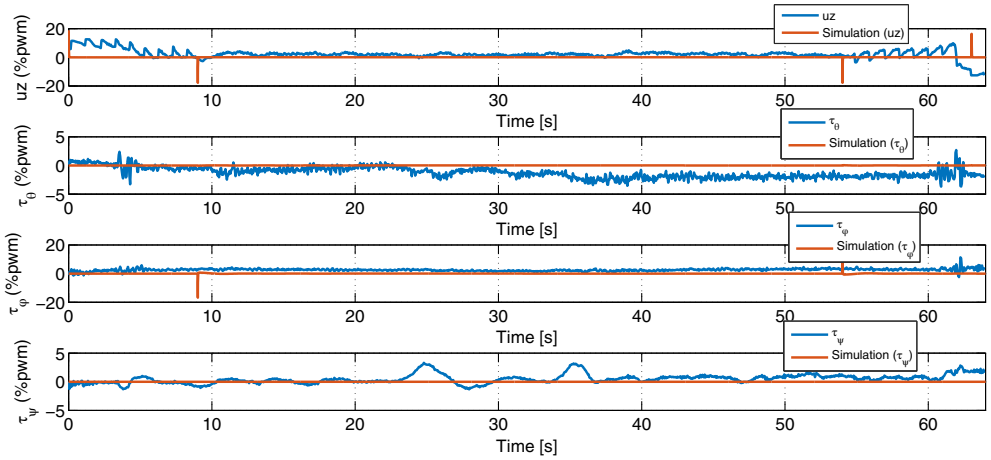

FIGURE 20 Control signal for the PD controllers with a trajectory tracking task, for outdoor flight [Colour figure can be viewed at wileyonlinelibrary.com]

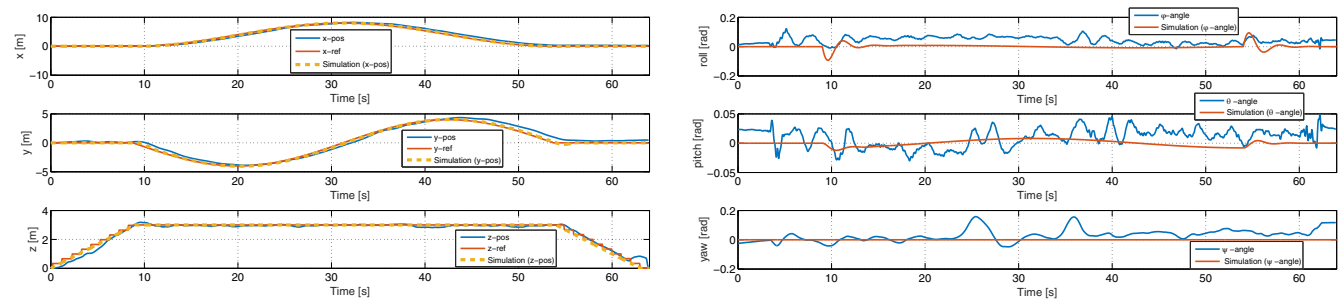

(A) Position of the vehicle

(B) Orientation of the vehicle

FIGURE 21 Position and orientation of the vehicle using PD controllers in a trajectory tracking task for outdoor flight [Colour figure can be viewed at wileyonlinelibrary.com]

Figure 22A,B displays the velocities for the variables x, y, and z and the orientation of the vehicle when PD controllers are used.

In Table 4, the data means for the 10 experiments made with each controller versus the simulation results for the trajectory tracking task are shown. The performance index $J_{u,\tau_\phi,\tau_\psi,\tau_\theta}$ was calculated adding the performance index values of J_u, J_{τ_ϕ}, J_{τ_θ}, and J_{τ_ψ} which are computed by $J_{control} = \sum(abs(Control(k)))$.

As can be seen in Table 4, the suboptimal nonlinear controller presents better performance respect to error, but it has a little more energy consumption than the optimal linear control. Of course, this feature depends directly from the selected penalization matrices, and the complexity of the suboptimal nonlinear controller. However, these data could give arguments to help to decide the selection of an specific optimized controller for the considered plant. In order to analyze the data dispersion of the errors for each set of experiments, we present the standard deviation of the error means in Table 5.

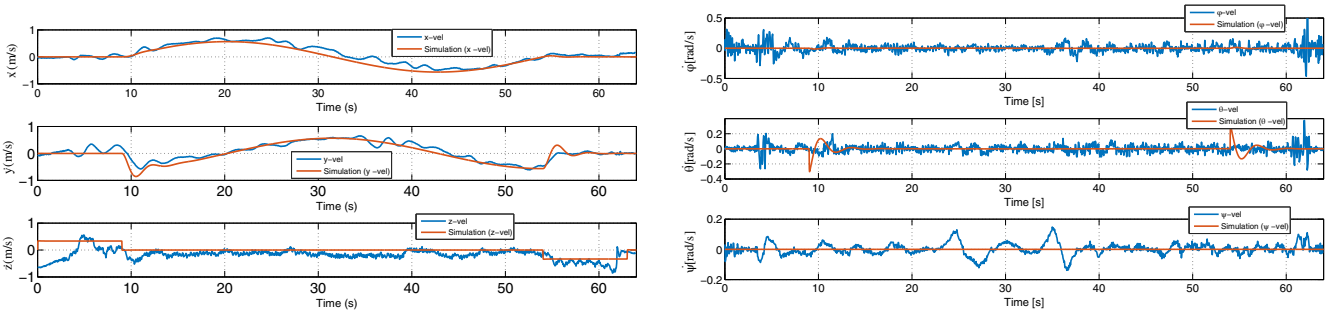

(A) Velocities of the vehicle

(B) Angular velocities of the vehicle

FIGURE 22 Velocities of the vehicle using PD controllers in a trajectory tracking task for outdoor flight [Colour figure can be viewed at wileyonlinelibrary.com]

TABLE 4 Comparative of performance and saving energy: Experimental and Simulation test, for trajectory tracking outdoor flight

Performance Index	$NLSOC_{exp}$	LOC_{exp}	PD_{exp}	$NLSOC_{simul}$	LOC_{simul}	PD_{simul}
$J_{u,\tau_\phi,\tau_\psi,\tau_\theta}$	5415.2	5374.5	6072.6	3165.5	1614	2269.3
J_e	1905.78	2332.04	2467.47	1351.7	1758.1	1549.13

TABLE 5 Comparative of error standard deviation: Experimental and Simulation tests, for the trajectory tracking task in outdoor flight

	$NLSOC_{exp}$	LOC_{exp}	PD_{exp}
Error Mean	0.19 m	0.23 m	0.3 m
Standard deviation	0.05	0.09	0.14

Similarly as previous task, the controller that induces a lower error mean is the suboptimal nonlinear controller with less dispersion but with a light higher energy consumption than the optimal linear controller.

6 | CONCLUSIONS

A suboptimal nonlinear control sequence is proposed for the finite horizon optimal control problem for nonlinear affine discrete systems. Notice that in order to obtain explicitly the controller, in each step an optimization procedure is used considering a quadratic performance index. Although the proposed controller is optimal in the local sense, the proposed method gives an alternative suboptimal solution to the open optimal control problem for nonlinear discrete systems. This proposed suboptimal nonlinear controller is experimentally contrasted with two controllers: linear discrete optimal control and nonoptimized PD controller. In outdoor environment, the experiments were made 10 times in order to demonstrate the feasibility of proposal and the repeatability of the results.

In fact, digital nonlinear suboptimal and linear optimal controllers with finite horizon were proposed in order to execute different tasks for a quadrotor. Experimental tests were conducted using a 4-DOF educational platform in indoor environment and a 6-DOF quadrotor in outdoor environment. In indoor flight, based on the experimental evidences, energy consumption of the nonlinear suboptimal controller is higher than the other controllers; however, the performance with respect to altitude error is better. The discrete linear optimal controller with exact linearization presents a similar error performance than a nonoptimized classic PD controller, but with the half of the energy consumption. For outdoor flight considering take off, hover, trajectory tracking, and landing tasks, the suboptimal nonlinear controller consumes a little more energy than the optimal linear controller and less energy than the nonoptimized PD controller, but it has a better performance than the optimal linear and PD controllers. Future works include to face up the min-max problem in order to reduce the effects of external disturbance or nonmodeled dynamics.

ORCID

Sergio Salazar https://orcid.org/0000-0002-5089-1791

REFERENCES

1. Ritz R, Hehn M, Lupashin S, D'Andrea R. Quadrocopter performance benchmarking using optimal control. Paper presented at: Proceedings of the 2011 IEEE International Conference on Intelligent Robots and System; 2011:5179-5186; San Francisco.
2. Liu H, Derawi D, Kim J, Zhong Y. Robust optimal attitude control of multirotors. Paper presented at: Proceedings of Australasian Conference on Robotics and Automation; 2013:1-6; Sydney, Australia.
3. Santoso F, Liu M, Egan G. Linear quadratic optimal control synthesis for a UAV. Paper presented at: Proceedings of the 12th Australian International Aerospace Congress; 2007; Melburne, Australia.
4. Tomić T, Moritz M, Sami H. Learning quadrotor maneuvers from optimal control and generalizing in real-time. Paper presented at: Proceedings IEEE International Conference on Robotics and Automation (ICRA), Hong Kong, China; 2014:1747-1754.
5. Chaudhari P. Aggressive maneuvers using differential flatness for a quadrotor; 2014. http://www.mit.edu/~pratikac/pub/chaudhari.aggressive.maneuver.pdf. octuber 2014.
6. Zawiski R, Blachuta M. Modelling and optimal control system design for quadrotor platform - an extended approach. *Bull Polish Acad Sci Techn Sci*. 2014;62(3):535-550.
7. Satici AC, Poonawala H, Spong MW. Robust optimal control of quadrotor UAV's. *IEEE Acces*. 2013;1:79-93.
8. Honglei A, Jie L, Jian W, Jianwen W, Hongxu M. Backstepping-based inverse optimal attitude control of quadrotor. *Int J Adv Robot Syst*. 2013;10(5):223.
9. Nuchkrua T, Parnichkun M. Identification and optimal control of quadrotor. *Thammasat Int J Sci Technol*. 2012;17(4):36-53.
10. Al-Younes YM, Al-Jarrah MA, Jhemi AA. Linear vs. nonlinear control techniques for a quadrotor vehicle. Paper presented at: Proceedings of the 7th International Symposium on Mechatronics and its Applications (ISMA10); April 20–22, 2010; Sharjah, UAE.
11. Adir VG, Stoica AM. Integral LQR control of a star-shaped octorotor. *Incas Bull*. 2012;4(2):3-18.
12. Tang YR, Li Y. Design of an optimal flight control system with integral augmented compensator for a nonlinear UAV helicopter. Paper presented at: Proceedings of the 10th World Congress on Intelligent Control and Automation; 2012:3927-3932; China.
13. Rodríguez-Guerrero L, Santos-Sánchez OJ, Cervantes-Escorcia N, Romero H. Real-time discrete suboptimal control for systems with input and state delays: experimental tests on a dehydration process. *ISA Trans*. 2017;71:448-457.
14. Zhang H, Qin C, Luo Y. Neural-network-based constrained optimal control scheme for discrete-time switched nonlinear system using dual heuristic programming. *IEEE Trans Automat Sci Eng*. 2014;11(3):839-849.
15. Mofid O, Mobayen S. Adaptive sliding mode control for finite-time stability of quad-rotor UAVs with parametric uncertainties. *ISA Trans*. 2018;72:1-14.
16. Mokhtari MR, Cherki B. A new robust control for minirotorcraft unmanned aerial vehicles. *ISA Trans*. 2015;56:86-101.
17. Zhang H, Qin C, Jiang B, Luo Y. Online adaptive policy learning algorithm for H_∞ state feedback control of unknown affine nonlinear discrete-time systems. *IEEE Trans Cybern*. 2014;44(12):2706-2718.
18. Zhang H, Feng T, Yang GH, Liang H. Distributed cooperative optimal control for multiagent systems on directed graphs: an inverse optimal approach. *IEEE Trans Cybern*. 2015;45(7):1315-1326.
19. Zhang S, Dong Y, Ouyang Y, Yin Z, Peng K. Adaptive neural control for robotic manipulators with output constraints and uncertainties. *IEEE Trans Neural Netw Learn Syst*. 2018;29(11):5554-5564.
20. He W, Meng T, He X, Ge SS. Unified iterative learning control for flexible structures with input constraints. *Automatica*. 2018;96:326-336.
21. Gao H, He W, Zhou C, Sun C. Neural network control of a two-link flexible robotic manipulator using assumed mode method. *IEEE Trans Ind Inform*. 2018.15(2):755–765.
22. Santos O, Romero H, Salazar S, Garca-Prez O, Lozano R. Optimized discrete control law for quadrotor stabilization: experimental results. *J Intell Robot Syst*. 2016;84(1–4):67-81.
23. Lin X, Huang Y, Cao N, Lin Y. Optimal control scheme for nonlinear systems with saturating actuator using ε-iterative adaptive dynamic programming. Paper presented at: Proceedings of the IEEE UKACC International Conference on Control (CONTROL), United Kingdom; 2012:58-63.
24. GrabCad Community https://grabcad.com/library/quadrotor-frame-1. Accessed octuber 8, 2016.
25. Castillo P, Lozano R, Dzul A. Stabilization of a mini rotorcraft with fours rotors. *IEEE Control Syst Mag*. 2005;25(6):45-55.
26. Castillo P, García P, Lozano R, Albertos P. Modelado y estabilización de un helicóptero con Cuatro Rotores. *Revista Ibereamericana de Automatica e Informática Industrial*. 2007;4(1):41-57.
27. Marconi L, Naldi R. Aggressive control of helicopters in presence of parametric and dynamical uncertainties. *Mechatronics*. 2008;18(7):381-389.
28. Bouabdallah S, Noth A, Siegwart R. PID vs LQ control techniques applied to an indoor micro quadrotor. Paper presented at: Proceedings of the Intelligent Robots and Systems Conference 2004 (IROS 2004), Sendai, Japan; vol. 3, 2004:2451-2456.
29. Bouabdallah S, Siegwart R. Full control of a quadrotor. In: 2007 IEEE/RSJ International Conference on Intelligent Robots and Systems. Ieee, San Diego California; 2007:153-158.
30. Bouabdallah S. Design and Control of Quadrotors with Application to Autonomous Flying (Doctoral dissertation). Ecole Polytechnique Federale de Lausanne; 2007.

31. Kirk DE. *Optimal Control Theory: An Introduction*. Dover Books on Electrical Engineering Series Englewood Cliffs, N.J. USA: Dover Publications; 2004.
32. Khalil HK. *Nonlinear Systems*. Upper Saddle River, NJ: Prentice Hall; 2002.

How to cite this article: Santos-Sánchez O, García O, Romero H, Salazar S, Lozano R. Finite horizon nonlinear optimal control for a quadrotor: Experimental results. *Optim Control Appl Meth*. 2020;1–27. https://doi.org/10.1002/oca.2662